Title

Nuclear Argonaute HRDE-1 Sustains Chromatin-Independent Transcriptional Silencing and Epigenetic Inheritance

Authors

Arantxa M. L. Rojas[1], Almira Chervova[1,2], Loan Bourdon[1], Jagannath Jayaraj[1,3], Ana Karina Morao[1], Olivier Feudjio[1], Sofija Illic[1], Sara Capurso[1], Piergiuseppe Quarato[1], Julie Ovieve[1], Germano Cecere[1#]

Affiliations

[1]Mechanisms of Epigenetic Inheritance, Department of Developmental and Stem Cell Biology, Institut Pasteur, CNRS UMR3738, Paris

[2]Bioinformatics and Biostatistics Hub, Department of Computational Biology, Institut Pasteur, USR 3756, CNRS, Paris

[3]Université Paris Cité, BioSPC, Paris, France

[#]Corresponding author: germano.cecere@pasteur.fr

Abstract

Epigenetic inheritance of transcriptional silencing is typically attributed to chromatin-based mechanisms in which Argonaute–small RNA complexes recruit histone-modifying enzymes. Here we show that, in *Caenorhabditis elegans*, the nuclear Argonaute HRDE-1 sustains germline repression independently of canonical heterochromatin marks. Inducible HRDE-1 depletion combined with germline nuclear sorting, CUT&Tag, and nascent transcription analysis revealed endogenous genes that become transcriptionally activated in the absence of HRDE-1 despite retention of H3K9me3 and H3K23me3. HRDE-1 further promotes polyUG-dependent amplification of antisense 22G-RNAs in perinuclear condensates, redefining nuclear Argonautes as active drivers of small RNA biogenesis rather than passive acceptors. Loss of HRDE-1 triggers progressive erosion of 22G-RNAs and prevents rapid re-establishment of silencing, underscoring the necessity of nuclear–cytoplasmic coupling for epigenetic memory. Our findings challenge the long-standing assumption that heterochromatin is required for transcriptional repression and redefine the mechanism by which nuclear Argonautes enforce epigenetic inheritance.

Introduction

Epigenetic inheritance of transcriptional silencing is widely attributed to chromatin-based repression[1] . In many systems, nuclear Argonaute proteins bound to small RNAs are thought to enforce this repression by recruiting histone-modifying enzymes, leading to deposition of repressive marks that can be stably transmitted across generations[2] . This model has shaped the prevailing view that heritable gene silencing requires canonical heterochromatin marks, yet whether such modifications are an obligate requirement for Argonaute-mediated silencing remains unresolved.

In *Caenorhabditis elegans*, small RNAs play a central role in transgenerational epigenetic inheritance. Exogenous double-stranded RNAs (dsRNAs) or endogenous PIWI-interacting RNAs (piRNAs) initiate the RNA-dependent RNA Polymerase (RdRP) transcription of antisense 22G-RNAs, which are loaded into Worm-specific Argonautes (WAGOs) to maintain silencing across generations[3] . The nuclear WAGO HRDE-1 (Heritable RNAi Deficient-1) is essential for this process[4] . Loss of HRDE-1 disrupts both dsRNA- and piRNA-triggered inheritance[4–6] . HRDE-1 activity has been associated with increased H3K9me3 and H3K23me3 at target loci[4,7–9], reinforcing the prevailing view that these histone modifications are required to maintain heritable RNA-mediated silencing.

Recent work has challenged this model. The inheritance of RNA interference (RNAi) initiated by double-stranded RNAs (dsRNAs) can persist in the absence of nuclear factors, relying instead on perinuclear condensates that propagate silencing via polyUGylated RNA templates and small RNA amplification[10,11] . Cytoplasmic factors such as ZNFX-1 and WAGOs can maintain silencing post-transcriptionally[10,11] , and in some cases silencing can continue even without the histone methyltransferases that deposit H3K9 and H3K23[12] . These findings raise the question of whether canonical heterochromatin marks are truly essential for HRDE-

1–mediated repression, or whether alternative heritable signals can substitute for chromatin modifications.

To address this, we combined inducible germline-specific depletion of HRDE-1 with nuclear sorting, CUT&Tag profiling of repressive histone modifications[13], and nascent transcription analysis[14]. This approach enabled direct comparison of transcriptional activity and chromatin state at HRDE-1 target loci with germline resolution. We show that HRDE-1 maintains transcriptional silencing of a defined set of endogenous genes without requiring canonical heterochromatin marks. Strikingly, some targets became transcriptionally active while retaining these repressive modifications, demonstrating that HRDE-1 can enforce transcriptional repression independently of chromatin state. Furthermore, we find that HRDE-1 couples nuclear repression to the transgenerational maintenance of antisense 22G-RNAs through amplification in perinuclear condensates. Together, these findings redefine the mechanism of nuclear Argonaute–mediated silencing and highlight small RNAs themselves as the primary heritable signal for a subset of germline targets.

Results

HRDE-1 is required in every generation to maintain germline gene silencing.

Most functional studies of HRDE-1 have relied on transgenic silencing reporters, which, while informative, may not capture the full range of endogenous targets. To systematically define HRDE-1–dependent repression of endogenous genes, we combined germline-specific auxin-inducible degradation (AID)[15] with genome-wide transcriptional profiling. Depletion of HRDE-1 using this system (**Fig. 1a** and **Extended Data Fig. 1a,b**) efficiently reduced protein levels (**Extended Data Fig. 1b**) and recapitulated the heritable RNAi defect of the *hrde-1* mutant in a GFP sensor assay (**Extended Data Fig. 1c**). We depleted HRDE-1 in one generation from the first to the last larval stage (G0) and maintained worms for four successive

100 generations in auxin (G4) (**Fig. 1a** and **Extended Data Fig. 1d**). At each generation,
101 synchronized L4-stage animals were collected using a COPAS Biosorter, as previously
102 described[6] , to ensure precise developmental staging across samples. Whole-worm RNA-seq
103 revealed that HRDE-1 depletion caused de-silencing of endogenous protein-coding and
104 pseudogenes in both G0 and G4 animals, while very few genes were downregulated (**Fig. 1b**),
105 indicating that we are primarily detecting genes directly repressed by HRDE-1. The total
106 number of misregulated genes was lower than in the *hrde-1* mutant[16], consistent with the degron
107 approach not fully depleting HRDE-1 protein. Importantly, the number of de-silenced genes
108 did not increase between G0 and G4 (**Extended Data Fig. 1f and Fig. 1c**), indicating that
109 HRDE-1 is required in each generation to maintain germline silencing, rather than having a
110 transgenerational effect.

111 HRDE-1 acts downstream of RNAi- or piRNA-triggered silencing to mediate
112 transcriptional repression. To compare its targets with those of PRG-1 (the *C. elegans* PIWI
113 Argonaute), we examined available RNA-seq to compare expression changes in *hrde-1*
114 *(tm1200)* and *prg-1 (n4357)* mutants[16] for the 69 HRDE-1–silenced genes (**Extended Data**
115 **Fig.1f**). Most of these genes were upregulated in *hrde-1* but not in *prg-1* mutants (**Fig. 1c,d**).
116 RT-qPCR confirmed that PRG-1 loss had little effect on these targets (**Fig. 1e**). In contrast,
117 mutation of NRDE-2, a nuclear silencing cofactor[4,17] , caused de-silencing to the same extent
118 as *hrde-1* (**Fig. 1e**), confirming that these genes are bona fide nuclear pathway targets. The fact
119 that these loci remain repressed by HRDE-1 in the absence of PRG-1 suggests they are distinct
120 from the spermatogenic targets identified in our previous study[6], which require piRNA trigger.
121 Consistent with this, RNA single-molecule fluorescence *in situ* hybridization (smFISH)[18] for
122 one of the most strongly upregulated genes, F07B7.1, showed robust expression throughout
123 the germline of *hrde-1* mutants but not in wild-type gonads (**Fig. 1f** and **Extended Data Fig.**
124 **1g**). HRDE-1 depletion from L1 to L4 recapitulated this pattern (**Fig. 1g** and **Extended Data**

125 **Fig. 1h**), demonstrating that repression requires HRDE-1 during germline development. This
126 broad expression pattern contrasts with piRNA-regulated spermatogenic genes, which are only
127 transiently expressed in pachytene nuclei[6], and supports the conclusion that these loci
128 represent a distinct class of constitutively silenced, HRDE-1–dependent targets. Therefore, this
129 defined gene set provides a tractable paradigm to dissect HRDE-1's mechanisms in small
130 RNA–mediated epigenetic inheritance.

131 **HRDE-1 depletion in G0 causes transcriptional de-silencing in germline nuclei.**

132 To confirm that these changes were germline-specific, we used a nuclear GFP reporter to
133 sort germline nuclei from HRDE-1–depleted worms (**Fig. 2a** and **Extended Data Fig. 2a-c**).
134 We performed nuclear RNA-seq and GRO-seq from these sorted nuclei, obtaining similar
135 number of de-silenced genes and very few downregulated, as we observe for the whole worm
136 RNA-seq (**Fig. 1**). Moreover, the high level of de-silencing detected with both approaches
137 strongly supports that these are nuclear targets of HRDE-1 (**Fig. 2b**), and that HRDE-1
138 maintains its transcriptional silencing every generation. We compared all the genes (n=364)
139 with significant changes (FDR $\leq$ 0.05) either in RNA-seq or GRO-seq from germline nuclei
140 and found that most of the genes present similar changes in both, total and nascent RNA levels
141 (**Fig. 2e**). Altogether, these results show that depleting HRDE-1 from L1 to L4 is sufficient to
142 transcriptionally de-silence its targets.

143 **HRDE-1 maintains silencing independently of canonical heterochromatin marks.**

144 Silencing by nuclear Argonautes is generally associated with deposition of repressive
145 histone marks[2,4,7–9]. To determine whether the transcriptional de-repression observed upon
146 HRDE-1 depletion results from loss of such marks, we developed a germline-specific
147 CUT&Tag approach by combining GFP-based germline nuclear sorting with histone
148 modification profiling, enabling high-resolution analysis of chromatin changes in the germline
149 (**Fig. 3a, Extended Data Fig. 2 and 3,** and **Methods**). This design overcomes two major

150 technical limitations of previous studies: (1) whole-worm profiling dilutes germline signals
151 with abundant somatic H3K9me3, masking germline-specific changes; and (2) the widely used
152 anti-H3K9me3 antibody (*Abcam 8898*) in *C. elegans* that was recently shown to cross-react
153 with other repressive marks (H3K27me3, H4K20me3)[19], potentially confounding
154 interpretation. We instead identified and validated an antibody with high specificity for
155 H3K9me3 in *C. elegans* (*Active Motif 39161*) (**Extended Data Fig. 2a-c**). As a critical test, we
156 depleted SET-25, the sole H3K9me3 methyltransferase in *C. elegans*[20], from the germline
157 between L1 and L4, which completely erased H3K9me3 peaks in sorted germline nuclei
158 (**Extended Data Fig. 2d,e**), confirming antibody specificity and the sensitivity of our
159 approach.

160 We next examined H3K9me3 at genes with changes by nuclear RNA-seq on the same
161 sorted germline nuclei upon HRDE-1 or SET-25 depletion (**Fig. 2b**, **Fig. 3a-c** and **Extended**
162 **Data Fig. 4c-e**). Of 140 upregulated genes, 80 and 75 overlapped with H3K9me3 peaks, with
163 72 showing no significant reduction in signal upon HRDE-1 depletion (**Fig. 3b,c**). Only three
164 genes exhibited both a loss of H3K9me3 and transcriptional upregulation (**Fig. 3c**). Moreover,
165 most of the downregulated genes upon HRDE-1 depletion have no changes in H3K9me3
166 (**Extended Data Fig. 4c-e**). Importantly, depleting SET-25 did not de-repress HRDE-1 target
167 genes (**Fig. 3d and Extended Data Fig. 4a,b**), indicating that H3K9me3 loss alone is
168 insufficient for transcriptional de-repression.

169 H3K23me3 is another heterochromatin mark implicated in HRDE-1–mediated
170 silencing[12]. HRDE-1 depletion caused more widespread changes for this mark, with 288 peaks
171 increased and 672 peaks reduced (**Fig. 3e** and **Extended Data Fig. 4f**). Among the 140
172 transcriptionally upregulated genes, 117 overlapped H3K23me3 peaks (**Fig. 3e**); of these, 56
173 showed reduced H3K23me3, three showed increases, and the majority exhibited no significant
174 change (**Fig. 3e,f**). Notably, the widespread loss of H3K23me3 did not correspond to broad

175 transcriptional upregulation (**Fig. 3e**), and increased deposition of this mark did not result in
176 transcriptional repression (**Extended Data Fig. 4g,h**), indicating that H3K23me3 changes are
177 largely uncoupled from gene expression in this context.

178 It has also been proposed that heritable transcriptional silencing could involve removal
179 of the active promoter mark H3K4me3, in addition to recruitment of repressive histone
180 modifiers[21] . To test this possibility, we profiled H3K4me3 in HRDE-1–depleted germline
181 nuclei. Only a modest number of H3K4me3 peaks were gained genome-wide (38 total), with
182 just 11 of 140 derepressed genes showing increased H3K4me3 (**Extended Data Fig. 4i–k**).
183 Moreover, the majority of upregulated genes did not overlap any H3K4me3 peak, indicating
184 that the observed transcriptional derepression cannot be explained by H3K4me3 accumulation.

185 Together, these results demonstrate that HRDE-1 maintains germline transcriptional gene
186 silencing independently of these histone modification marks, and suggest that deposition of
187 repressive chromatin modifications is a downstream consequence of transcriptional silencing
188 rather than its primary cause. Importantly, several HRDE-1 targets were robustly de-repressed
189 while still retaining wild-type levels of H3K9me3 and/or H3K23me3, demonstrating that
190 transcription can proceed even in the presence of canonical repressive histone modifications.

191 **HRDE-1 promotes the transgenerational maintenance of 22G-RNAs.**

192 Having established that HRDE-1 sustains transcriptional silencing without canonical
193 heterochromatin marks, we next investigated whether its function is instead linked to
194 maintaining the small RNA populations required for transgenerational silencing. Loss of
195 HRDE-1 has previously been associated with large-scale changes in small RNA levels,
196 particularly antisense 22G-RNAs[16]. Artificial HRDE-1 tethering can also trigger *de novo*
197 production of heritable small RNAs[22], suggesting a direct role in promoting their biogenesis.

198 We sequenced small RNAs from G0, G1, G2, and G4 HRDE-1–depleted L4 worms (**Fig.
199 4a,b** and **Extended Data Fig. 5a**). Across generations, we predominantly observed a reduction

200 in antisense 22G-RNAs, with the extent of dysregulation increasing gradually (**Fig. 4b**). The
201 progressive nature of this effect suggests that it cannot be explained solely by reduced stability
202 of existing small RNAs, but rather reflects a transgenerational requirement for HRDE-1 in
203 promoting 22G-RNA biogenesis.

204 Although 22G-RNAs were also reduced in G0 animals, none of the 69 genes consistently
205 de-silenced upon HRDE-1 depletion (**Extended Data Fig. 1f** and) showed decreased 22G-
206 RNAs (**Fig. 4c** and **Extended Data Fig. 5b,c**). Thus, in the early generation, transcriptional
207 de-repression can occur without detectable changes in small RNA levels, and conversely, small
208 RNA changes do not necessarily correspond to transcriptional changes (**Fig. 4c** and **Extended**
209 **Data Fig. 5b,c**). This also suggests that the 22G-RNAs available for loading into other WAGOs
210 in G0 HRDE-1-depleted animals is insufficient to compensate for the lack of HRDE-1 and
211 maintain repression post-transcriptionally, as previously observed[10] .

212 The number of genes losing 22G-RNAs increased markedly across generations (**Fig. 4a,b**
213 and **Extended Data Fig. 5b**), in contrast to the number of de-silenced genes, which remained
214 stable (**Fig. 1a,b**). By G4, 22 of the 69 de-silenced genes had significantly reduced antisense
215 22G-RNAs in both replicate experiments (**Extended Data Fig. 5c**). These genes showed no
216 change in 22G-RNAs in G0 but a strong reduction in G4, with a gradual decline across
217 generations (**Fig. 4d**), as also shown for F15D4.5 as an example (**Fig. 4e**). These observations
218 indicate that HRDE-1 has two separable roles: direct transcriptional silencing and maintenance
219 of 22G-RNA populations across generations.

220 **Mutator foci, but not Z granules, are required for HRDE-1–dependent 22G-RNA**
221 **biogenesis and transcriptional repression.**

222 To dissect the cytoplasmic requirements for HRDE-1–dependent silencing, we began by
223 testing whether its targets require polyUGylation, a key step in 22G-RNA biogenesis that
224 follows endonucleolytic cleavage of mRNA targets and is catalyzed by the polymerase RDE-

225 3[23]. For several HRDE-1 targets with transgenerational 22G-RNA loss, polyUGylation in *hrde-*
226 *1* mutants was as impaired as in *rde-3* mutants (**Fig. 5a**), indicating a strong defect in this step
227 of small RNA amplification. This contrasts with previous findings[6] showing that
228 polyUGylation of spermatogenic genes triggered by piRNAs is independent of HRDE-1 (e.g.,
229 D2096.1 and F55A6.3), suggesting that most HRDE-1 targets identified here do not require
230 piRNAs to initiate 22G-RNA biogenesis but do require HRDE-1 to sustain polyUGylation and
231 22G-RNA accumulation.

232 We next tested the involvement of the NYN domain-containing endonucleases RDE-8,
233 NYN-1, and NYN-2 acting upstream of polyUGylation[23,24]. PolyUGylation impairment in
234 *hrde-1* mutants mirrored that observed in *rde-8* mutants or *nyn-1;nyn-2* double mutants (**Fig.**
235 **5b**). Consistent with this, expression levels of HRDE-1 target genes in *rde-8;nyn-1;nyn-2* triple
236 mutants ("endo") were comparable to *hrde-1* mutants (**Fig. 5c**).

237 Given this dependence on core cytoplasmic biogenesis factors, we asked whether HRDE-
238 1–dependent 22G-RNA production requires specific perinuclear condensates. Loss of MUT-
239 16, an essential scaffold for Mutator foci that house RDE-3, RDE-8, and other 22G-RNA
240 amplification factors[25] , phenocopied *hrde-1* mutants, causing similar de-silencing of HRDE-1
241 targets (**Fig. 5c**). These results indicate that Mutator foci are essential for both the cytoplasmic
242 biogenesis and the transcriptional repression of HRDE-1 targets, providing the key interface
243 between nuclear Argonaute activity and small RNA amplification.

244 Given the established role of Z granules in cytoplasmic post-transcriptional
245 silencing[10,26] , we next asked whether they contribute to the maintenance of endogenous
246 HRDE-1–mediated transcriptional repression. Z granules are perinuclear condensates
247 nucleated by the helicase ZNFX-1[26]. ZNFX-1 cooperates with cytoplasmic Argonautes to
248 sustain RNAi inheritance and to maintain silencing in the absence of nuclear HRDE-1, acting
249 through polyUGylated RNA templates and small RNA amplification[10,11]. We therefore tested

250 whether ZNFX-1 is similarly required for HRDE-1–regulated endogenous targets. Publicly
251 available small RNA-seq data[10] together with our polyUGylation assays revealed that *znfx-1*
252 mutants have a substantial reduction in 22G-RNAs and impaired polyUGylation for several
253 HRDE-1-regulated genes (**Extended Data Fig. 6a–c**), similar to *hrde-1* mutants. Notably,
254 however, RT-qPCR, and smFISH all showed only mild or no transcriptional derepression of
255 these targets in *znfx-1* mutants compared to wild type (**Fig. 5c,d** and **Extended Figure 6d**).
256 Moreover, combined loss of HRDE-1 and ZNFX-1 did not enhance derepression in either G0
257 or G1 (**Fig. 5e,f and Extended Fig. 6e**).

258 Thus, although Z granules influence the abundance of small RNAs for HRDE-1 targets,
259 they are not required to maintain transcriptional repression. Unlike RNAi inheritance, Z
260 granules do not provide a compensatory cytoplasmic pathway for these HRDE-1 targets, which
261 relies selectively on Mutator foci to couple transcriptional repression with heritable small RNA
262 amplification.

263 **Silencing recovery mediated by HRDE-1 requires 22G-RNAs.**

264 By applying inducible depletion of HRDE-1, we uncovered the dynamics of silencing
265 maintenance across generations. We next investigated how silencing is re-established once
266 HRDE-1 expression is restored. Worms depleted of HRDE-1 for four generations (G4) were
267 removed from auxin treatment and propagated to the first (R1), fourth (R4), and sixth (R6)
268 generations before collection at the L4 stage (**Fig. 6a** and **Extended Data Fig. 1a,d,e**). Notably,
269 whereas depleting HRDE-1 during germline development (G0) was sufficient to de-silence
270 these genes (**Fig. 1** and **Fig. 6b,c**), re-expressing HRDE-1 during the same developmental
271 period failed to restore repression (**Fig. 6b,c**). RNA-seq analysis revealed that ~50% of the 69
272 protein-coding and pseudogenes de-silenced in G4 remained strongly upregulated in R1 (**Fig.
273 6b**). Instead, silencing was gradually re-established over several generations, with some genes
274 remaining de-silenced even at R6 (**Fig. 6b,c**).

275 Since most targets showed a pronounced loss of antisense 22G-RNAs by G4, we next
276 assessed 22G-RNA levels during recovery. In R1, failure to restore silencing correlated with a
277 complete lack of 22G-RNA recovery, indicating that HRDE-1 requires these small RNAs to
278 act in transcriptional repression (**Fig. 6b,c**). In later generations, 22G-RNAs progressively
279 returned, paralleling transcriptional repression, consistent with the idea that their restoration,
280 like their maintenance, is transgenerationally promoted by HRDE-1.

281 To determine whether recovery depends on the same cytoplasmic biogenesis steps
282 required for maintenance, we monitored polyUGylated RNA intermediates for two HRDE-1
283 targets with distinct recovery kinetics, F15D4.5 and C38D9.2 (**Fig. 6c,d**), alongside a piRNA
284 target (*bath-13*) whose 22G-RNA accumulation are HRDE-1–independent[6] (**Extended Data**
285 **Fig. 7a**). The polyUGylation of *bath-13* remained unchanged across all generations, whereas
286 F15D4.5 and C38D9.2 showed a strong G4 reduction resembling *hrde-1* mutants and no
287 improvement in R1 (**Fig. 6c,d** and **Extended Data Fig. 7a**). PolyUG signal increased by R4
288 and R6, although for C38D9.2 the pattern remained weaker and more discrete than in controls,
289 matching its slower transcriptional recovery. These results suggest that gene-specific
290 differences in HRDE-1 efficiency at promoting polyUGylation underlie variable silencing
291 restoration rates, echoing earlier observations[12].

292 Finally, to directly test whether recovery failure in R1 is caused by small RNA depletion,
293 we repeated the experiment with shorter HRDE-1 depletion (G0) (**Fig. 6e**). Since 22G-RNA
294 levels are unaffected in G0 for de-silenced genes, we predicted that restoring HRDE-1 in the
295 next generation would enable immediate repression. Indeed, small RNA sequencing in R1 and
296 R2 after G0 depletion confirmed wild-type 22G-RNA levels (**Fig. 6e**), and RT-qPCR showed
297 that repression was re-established in R1 (**Fig. 6f** and **Extended Data Fig. 7b**). This
298 demonstrates that silencing recovery by HRDE-1 strictly depends on the presence of target-

299 matching 22G-RNAs and that their biogenesis, once lost, must be rebuilt over multiple
300 generations.
301
302 **Discussion**
303 By combining inducible germline depletion of HRDE-1 with a method we developed to
304 isolate and profile sorted germline nuclei (see methods), we captured both immediate and
305 transgenerational consequences of nuclear Argonaute loss with temporal resolution that
306 conventional mutants cannot provide. A key technical advance was the application of germline
307 CUT&Tag with a validated H3K9me3 antibody, which overcomes two limitations of previous
308 studies: masking of germline signals in whole-worm assays and the use of non-specific
309 antibodies[19]. This approach enabled direct, high-resolution interrogation of the chromatin state
310 at HRDE-1 targets.
311 This approach allowed us to identify a set of endogenous genes whose repression depends
312 exclusively on HRDE-1 and to dissect two distinct modes of silencing: (1) maintaining
313 transcriptional repression independently of canonical heterochromatin marks, and (2)
314 promoting the transgenerational maintenance of 22G-RNAs through polyUG-dependent
315 amplification in Mutator foci.
316 **Chromatin independence of HRDE-1–mediated silencing**
317 Our data reveal that HRDE-1 maintains transcriptional silencing without reliance on
318 canonical heterochromatin. Most HRDE-1–derepressed targets retain wild-type levels of
319 H3K9me3 and/or H3K23me3, and loss of either or both modifications has no impact on their
320 repression. This challenges the prevailing model, based largely on genetic evidence[12,27], that
321 nuclear Argonautes sustain silencing by recruiting histone methyltransferases. Instead, our
322 results support a model in which repressive marks are deposited downstream of HRDE-1–
323 mediated repression. We also considered whether derepression could be explained by changes

324 in the active promoter mark H3K4me3, which has been proposed to contribute to heritable
325 silencing[21] . However, H3K4me3 gains were modest and affected only a minority of
326 derepressed genes, indicating that promoter activation in this context is not driven by canonical
327 active chromatin marks.

328 Consistent with this model, no direct interaction between HRDE-1 and histone
329 methyltransferases has been detected[28]. In contrast, proteomic analyses have identified RNA
330 polymerase II subunits among HRDE-1–associated factors[28], raising the possibility that
331 HRDE-1 influences transcription directly. Our GRO-seq data are consistent with this view:
332 HRDE-1 loss leads to increased nascent transcription, ruling out a model based solely on
333 nuclear transcript degradation and suggesting impaired Pol II recruitment or initiation. Notably,
334 this differs from the mechanism described for the somatic nuclear Argonaute NRDE-3, which
335 inhibits Pol II during elongation[29]. Together, these findings indicate a distinct mode of
336 repression by HRDE-1 in the germline and revise the current model of nuclear Argonaute
337 function.

338 **A distinct, piRNA-independent class of HRDE-1 targets.**

339 The genes derepressed upon HRDE-1 loss differ from previously characterized
340 spermatogenic targets, which are silenced anew each generation downstream of piRNAs and
341 PRG-1[6]. In contrast, the genes we identify are constitutively repressed in the germline and
342 remain silenced in every generation under normal conditions. We propose that their silencing
343 may have originated from ancestral piRNA targeting but no longer requires ongoing piRNA
344 input, leaving HRDE-1 as the sole factor responsible for their repression. Consistent with this,
345 antisense 22G-RNAs for these genes are unaffected or even increased in *prg-1* mutants,
346 reminiscent of the hyper-amplification of small RNAs triggered by RNAi in this background,
347 which can perpetuate silencing indefinitely[30]. This distinct group of HRDE-1-dependent loci

348 therefore represents a paradigm of Argonaute-mediated repression that is self-sustaining and
349 independent of piRNA input.

350 **Coupling nuclear silencing to cytoplasmic 22G-RNA amplification.**

351 Our results show that HRDE-1 sustains transgenerational silencing not through stable
352 chromatin imprints, but by maintaining antisense 22G-RNA populations via polyUG-
353 dependent amplification in Mutator foci. This continual replenishment is essential, since
354 repression is rapidly lost in its absence. Thus, nuclear target recognition by HRDE-1 is coupled
355 to cytoplasmic small RNA biogenesis, ensuring that small RNAs themselves, rather than
356 heterochromatin, serve as the heritable memory.

357 Mechanistically, HRDE-1–dependent 22G-RNA biogenesis requires RDE-8/NYN-1/2–
358 mediated cleavage, RDE-3–mediated polyUGylation, and intact Mutator foci (MUT-16), but
359 not Z granules. This argues against the idea that HRDE-1 promotes small RNA amplification
360 in the nucleus[10], instead supporting a strictly cytoplasmic process. Although the Z granule
361 helicase ZNFX-1 has been implicated in nuclear-independent RNAi inheritance[11] and, in some
362 contexts, shown to act redundantly with HRDE-1[10] , we find it is not required here: *znfx-1*
363 mutants display reduced 22G-RNAs at HRDE-1 targets but no transcriptional de-repression,
364 and combined loss of HRDE-1 and ZNFX-1 does not enhance defects. These results challenge
365 the view that cytoplasmic Argonautes can broadly compensate for nuclear silencing, and
366 instead re-establish HRDE-1 as central to transgenerational inheritance.

367 **Small RNAs as the heritable memory of repression.**

368 Our depletion–recovery experiments revealed that HRDE-1 requires pre-existing small
369 RNAs to re-establish silencing. After four generations without HRDE-1, repression was
370 restored only gradually across multiple generations, in parallel with the slow re-accumulation
371 of 22G-RNAs. By contrast, short-term depletion (one generation) left small RNA levels intact
372 and allowed immediate recovery. Recovery dynamics also varied between targets: for example,

the paralogs *F15D4.5* and *C38D9.2* displayed distinct resilience, likely reflecting differences in polyUGylation efficiency and sequence complementarity. These findings demonstrate that heritable silencing depends not on a persistent chromatin state, but on the continuous availability of small RNAs to guide HRDE-1.

Broader implications for chromatin and transgenerational inheritance.

Our findings establish HRDE-1 as a central integrator of nuclear transcriptional repression and cytoplasmic small RNA amplification, operating independently of canonical heterochromatin marks. The observation that transcription can be reactivated despite the continued presence of H3K9me3 and H3K23me3 parallels rare cases in *S. pombe* [31], where transcriptional changes occur without loss of repressive chromatin, and in *Drosophila*[32], where specialized transcriptional machinery drives piRNA cluster expression within a heterochromatic environment. By extending this paradigm to the germline of *C. elegans*, our GRO-seq results suggest that a nuclear Argonaute can repress transcription at the level of Pol II recruitment, indicating that chromatin marks are not always the decisive signal for transcriptional control.

More broadly, these results redefine how nuclear Argonautes sustain transgenerational gene silencing: by coupling nuclear recognition of targets with continual small RNA replenishment in cytoplasmic condensates, ensuring that small RNAs — rather than chromatin imprints — serve as the heritable memory. By showing that transcriptional derepression occurs independently of both repressive (H3K9me3, H3K23me3) and active (H3K4me3) histone marks, our work compels a re-evaluation of the long-standing assumption that chromatin is the central medium of epigenetic inheritance, and highlights nuclear Argonautes as active drivers of small RNA-based epigenetic memory across generations.

400 **Figures and Extended Data Figures.**
401
402 **Fig. 1: HRDE-1 is required in every generation to maintain germline gene silencing. a**,
403 Schematic of worm cultivation for transcriptome profiling. HRDE-1 was depleted in the
404 germline using an auxin-inducible degron from L1 to L4 (G0) or continuously for four
405 generations (G4), followed by total RNA-seq from whole worms. **b,** MA-plot showing $\log_2$
406 fold change versus mean expression in G0 and G4 samples for protein-coding and
407 pseudogenes. Upregulated genes are shown in orange ($\log_2$FC ≥ 1, FDR ≤ 0.05); downregulated
408 genes in blue ($\log_2$FC ≤ –1, FDR ≤ 0.05). n = 2 biological replicates. **c**, Box plot of $\log_2$ fold
409 change (FC) in RNA-seq for the 68 upregulated genes in G0 and G4 (**see Extended Data Fig.**
410 **1f**), and their changes in *hrde-1* and *prg-1* mutants (Barucci et al., 2020). **d,** Genome browser
411 views of representative targets, showing RNA-seq for HRDE-1-depleted (control, blue;
412 HRDE-1 depletion, red) and *hrde-1* or *prg-1* mutants (WT, grey; *hrde-1*, green; *prg-1*, pink).
413 TE = mapped transposable elements. Data are averaged from two biological replicates. **e**, RT–
414 qPCR validation of selected HRDE-1–regulated genes in *hrde-1*, *prg-1*, and *nrde-2* mutants at
415 the L4 stage, normalized to *act-3*. Bars show mean $\log_2$FC; dots represent individual replicates
416 (n = 3). **f**, **g**, RNA FISH for F07B7.1 (magenta) in L4 stage *hrde-1* mutants (**f**) or HRDE-1–
417 depleted G0 worms (**g**) compared to controls. DAPI (cyan) marks nuclei; gonads are outlined
418 with dashed white lines. Details of the two areas outlined in yellow are shown below for each
419 gonad. Corresponding single-channel images are in **Extended Data Fig. 1g,h**.
420 **Fig. 2: De-silencing in G0 HRDE-1-depleted germline nuclei is transcriptional. a,**
421 Schematic of germline nuclei isolation after HRDE-1 depletion for RNA-seq and GRO-seq
422 analysis. **b, c,** MA-plot showing $\log_2$ fold change versus mean expression in G0 for protein-
423 coding and pseudogenes in RNA-seq (**b**) and GRO-seq experiments (**c**). Upregulated genes are
424 shown in orange ($\log_2$FC ≥ 1, FDR ≤ 0.05); downregulated genes in blue ($\log_2$FC ≤ –1, FDR ≤
425 0.05). n = 4 biological replicates **d,** Genome browser views of representative targets, showing

426 RNA-seq and GRO-seq for G0 HRDE-1-depleted (control, blue; HRDE-1 depletion, red)
427 germline nuclei, RNA-seq from G0 whole worm (as in **Fig. 1d**), and RNA-seq and GRO-seq
428 from whole worms *hrde-1* mutants are included for comparison (WT, grey; *hrde-1*, green)
429 (Data from Barucci et al., 2020 and Cornes et al., 2022). TE = mapped transposable elements.
430 Data are averaged from two or four biological replicates. **e,** Heatmap summarizing significant
431 expression changes (FDR ≤ 0.05) for HRDE-1–silenced genes in G0 HRDE-1–depleted
432 germline nuclei in RNA-seq or GRO-seq.

433 **Fig. 3: HRDE-1 maintains silencing independently of canonical heterochromatin marks.**
434 **a**, Schematic of germline nuclei isolation after HRDE-1 depletion for histone modification
435 profiling by CUT&Tag. **b**, MA-plot of H3K9me3 CUT&Tag signal in G0 germline nuclei after
436 HRDE-1 depletion. Genes upregulated in G0 HRDE-1–depleted nuclei (from **Fig. 2b**) that
437 intersect H3K9me3 peaks are shown in orange; significantly reduced H3K9me3 peaks are in
438 dark grey. n = 4 biological replicates. **c**, Box plot of $\log_2$ fold change (FC) for upregulated genes
439 from G0 HRDE-1–depleted germline nuclei (**Fig. 2b**) intersecting with H3K9me3 peaks.
440 Categories: ns (no significant change but H3K9me3 peak present), no peak, or DOWN
441 (significantly reduced H3K9me3). **d**, RT–qPCR validation of selected genes in HRDE-1–
442 depleted (green) or SET-25–depleted (pink) L4 germlines, normalized to *act-3*. Bars show
443 mean $\log_2$FC; dots indicate biological replicates. Bars below indicate $\log_2$FC of H3K9me3 peak
444 signal for each gene; "na" = no detected peak. **e**, MA-plot of H3K23me3 CUT&Tag signal in
445 G0 germline nuclei after HRDE-1 depletion, with color coding as in (**b**). n = 4 biological
446 replicates. **f**, Box plot of $\log_2$FC for upregulated genes from G0 HRDE-1–depleted germline
447 nuclei (**Fig. 2b**) intersecting with H3K23me3 peaks. Categories as in (**c**).

448 **Fig. 4: HRDE-1 is required for transgenerational maintenance of 22G-RNAs. a,**
449 Experimental design for small RNA-seq across generations following germline HRDE-1
450 depletion. HRDE-1 was depleted during development (G0) or continuously for one (G1), two

451 (G2), or four (G4) generations. **b**, MA-plot of antisense 22G-RNAs mapping to protein-coding
452 and pseudogenes in HRDE-1–depleted versus control worms. Orange = significantly increased
453 22G-RNAs ($\log_2$FC ≥ 1, FDR ≤ 0.05), blue = significantly decreased 22G-RNAs ($\log_2$FC ≤ –
454 1, FDR ≤ 0.05). n = 2 biological replicates. **c**, Genome browser view of F15D4.5, a
455 representative HRDE-1 target. mRNA expression is similarly de-silenced in G0 and G4 (top;
456 RNA-seq, from **Fig. 1b**), whereas 22G-RNAs are reduced only in G4 (bottom). Control = blue,
457 HRDE-1 depletion = red. TE = mapped transposable elements. **d**, Box plot of $\log_2$ fold change
458 (FC) at G0, G1, G2, and G4 in antisense 22G-RNAs for 21 HRDE-1-silenced genes that lose
459 small RNAs in G4 (**see Extended Data Fig. 5c**). **f**, Genome browser view showing gradual,
460 generation-dependent reduction of antisense 22G-RNAs at F15D4.5. Control = blue, HRDE-1
461 depletion = red. TE = mapped transposable elements.

462 **Fig. 5: Mutator foci, but not Z granules, are required for HRDE-1–dependent 22G-RNA**
463 **biogenesis and transcriptional repression. a**,**b**, PolyUGylation assay for HRDE-1–silenced
464 genes that lose 22G-RNAs transgenerationally in different genetic backgrounds. The gene *gsa-*
465 *1* is included as a control. **c**, RT–qPCR analysis of HRDE-1–silenced genes in *hrde-1*, *rde-*
466 *8;nyn-1;nyn-2* triple mutants ("endo"), *mut-16* and *znfx-1* mutants at the L4 stage. Expression
467 values are normalized to *act-3*. Bars represent mean $\log_2$ fold change (FC), dots indicate
468 biological replicates (n = 3). **d**, RNA FISH for F07B7.1 (magenta) in L4-stage wild-type, *hrde-*
469 *1*, *znfx-1*, and *hrde-1;znfx-1* mutants. DAPI (cyan) marks nuclei; gonads are outlined with
470 dashed white lines. e, RT–qPCR analysis of selected HRDE-1-silenced genes as in HRDE-1-
471 depleted G0 and G1 worms at the L4 stage in control and *znfx-1* mutant backgrounds,
472 normalized to *act-3*. Bars show mean $\log_2$FC; dots represent biological replicates (n = 5). In
473 **Extended Data Fig. 6d**, the expression changes in *znfx-1* and wild-type worms grown in
474 control or auxin are shown.

475 **Fig. 6: HRDE-1 silencing maintenance requires 22G-RNA biogenesis.** **a**, Experimental
476 design to assess transgenerational maintenance and recovery of HRDE-1–dependent silencing.
477 **b**, Heatmap summarizing expression and 22G-RNA changes for the 69 HRDE-1–silenced
478 genes (from **Fig. 1b**) in G0 and G4 HRDE-1–depleted worms (red) and in R1, R4, and R6
479 generations after HRDE-1 re-expression (purple). **c**, Genome browser views of representative
480 genes: F15D4.5 and C38D9.2 (HRDE-1 targets) showing RNA-seq and 22-RNAs changes.
481 Control samples are in blue, HRDE-1 depletion in red, and recovery in purple. TE = mapped
482 transposable elements. **d**, PolyUGylation assay for F15D4.5 and C38D9.2 across control
483 (blue), G0 and G4 depletion (red), and R1, R4, and R6 recovery generations (purple). *gsa-1*
484 serves as a control. **e**, Top: Experimental design testing silencing recovery after one (G0) or
485 four (G4) generations of depletion. Bottom: Genome browser snapshots showing 22G-RNA
486 levels for F15D4.5 and C38D9.2 in control (blue), depletion (red, G0), and recovery (purple,
487 R1 and R2). **f**, RT–qPCR analysis of selected genes in G0, R1, and R2 worms at the L4 stage,
488 normalized to *act-3*. Bars show mean $\log_2$FC; dots represent biological replicates (n = 3–5).
489 Bottom: corresponding average fold change of 22G-RNAs for each gene across generations.
490 **Extended Data Fig. 1: Validation of the auxin-inducible degron system and experimental**
491 **setup for HRDE-1 depletion and recovery. a**, Schematic of the auxin-inducible degron (AID)
492 strategy for HRDE-1 depletion in the germline. **b**, Western blot of AID::3xFLAG::HRDE-1 in
493 wild-type (untagged HRDE-1) and AID-tagged strains with or without germline TIR1, in the
494 presence or absence of auxin. Anti-FLAG antibody was used for detection; GAPDH served as
495 a loading control. **c**, RNAi inheritance assay in AID::3xFLAG::HRDE-1; GFP::piRNA sensor
496 worms injected with dsRNA against GFP and developed on ethanol (control) or auxin (HRDE-
497 1 depleted). Silencing was monitored in the F1 generation. **d**, Stage distribution of L4 larvae
498 sorted with COPAS used for RNA-seq and small RNA-seq in **Fig. 1a,b**, **Fig. 6a-d**, and
499 **Extended Data Fig. 4b,c**. **e**, Western blot of L4 larvae at G0 and G4 (HRDE-1 depleted, red)

500 and R1 (recovery, purple), compared to control (blue). Two biological replicates used for
501 sequencing are shown (replicates 3 and 4). **f**, Venn diagram showing the intersection between
502 G0 and G4 upregulated genes (FDR <= 0.05 and log2FC >=1) from RNA-seq of HRDE-1
503 depleted worms (**Fig. 1b**). **g,h**, Corresponding single-channel images of RNA FISH shown in
504 **Fig. 1 f,g.**

505 **Extended Data Fig. 2: Set up for germline nuclei isolation from HRDE-1-depleted worms.**
506 **a,** Schematics showing the preparation of HRDE-1-depleted germline nuclei for downstream
507 approaches (Corresponding to **Figs. 2 and 3**). **b,** Western blot of L4 lysates corresponding to
508 samples used in **Fig. 2** to test HRDE-1 depletion in each replicate (n = 4 biological replicates).
509 **c,** Record examples of nuclei sorting using FACS, P4 is the sorting gate for GFP-positive
510 nuclei.

511 **Extended Data Fig. 3: Setup for H3K9me3 analysis using CUT and Tag in sorted germline**
512 **nuclei. a,** Genome browser views of a representative region in Chromosome V, showing CUT
513 and Tag results using four different antibodies to detect H3K9me3 in wild-type and *met-2;set-*
514 *25* L4 worms. **b,** Genome browser views of the same representative region as in **a**, showing
515 CUT and Tag results using the Active Motif antibody to detect H3K9me3, with addition of
516 synthetic nucleosomes (spike-in, Epicypher) in wild-type and *met-2;set-25* sorted L4 worms.
517 Coverage normalized by Counts per million or using spike-in scaling factors is shown. **c,**
518 Antibody specificity table for H3K9me3 antibody corresponding to the experiment shown in
519 **b**. **d,** Schematics showing the preparation of SET-25-germline-depleted germline nuclei for
520 CUT and Tag to assess changes in H3K9me3. On the right, MA plot showing H3K9me3
521 changes upon SET-25 depletion (G0). **g,** Genome browser views of the same representative
522 region as in **a**, showing CUT and Tag results using the Active Motif antibody to detect
523 H3K9me3 in germline nuclei depleted for SET-25 (G0) and control from the experiment shown
524 in **d**. The coverage was normalized using a spike-in-derived scaling factor.

525 **Extended Data Fig. 4: HRDE-1 maintains gene silencing independently of canonical**
526 **histone modifications. a**, MA-plot of H3K9me3 CUT&Tag signal in germline nuclei upon
527 SET-25 depletion with orange highlighting genes upregulated in HRDE-1–depleted nuclei
528 (**Fig. 2b**) that intersect H3K9me3 peaks. b, Same as in **a**, but with blue highlighting genes
529 downregulated in HRDE-1–depleted nuclei. **c**, MA-plot of H3K9me3 signal upon HRDE-1
530 depletion (G0). **d**, Same as (**c**), highlighting genes downregulated in HRDE-1–depleted nuclei
531 (**Fig. 2b**) that intersect H3K9me3 peaks. **e**, Box plot of $\log_2$ fold change (FC) for downregulated
532 genes from HRDE-1–depleted germline nuclei grouped by H3K9me3 status: ns (no significant
533 change, peak present), no peak, or DOWN (significantly reduced peak). **f**, MA-plot of
534 H3K23me3 signal upon HRDE-1 depletion (G0). **g**, Same as **f**, with blue highlighting
535 downregulated genes intersecting H3K23me3 peaks. **h**, Box plot of $\log_2$FC for downregulated
536 genes from HRDE-1–depleted germline nuclei grouped by H3K23me3 status. **i**, MA-plot of
537 H3K4me3 signal upon HRDE-1 depletion (G0). **j**, Same as **i**, with orange highlighting
538 upregulated genes intersecting H3K4me3 peaks. **k**, Same as **i**, with blue highlighting
539 downregulated genes intersecting H3K4me3 peaks.
540 **Extended Data Fig. 5: Transgenerational dynamics of 22G-RNAs upon HRDE-1**
541 **depletion. a**, Schematic of worm cultivation for small RNA analysis and Western blot
542 confirming HRDE-1 depletion in sorted L4 larvae used for library preparation, corresponding
543 to samples used in **Fig. 4b**. **b**, MA-plot of antisense 22G-RNA levels in G0 and G4 worms.
544 Orange = upregulated 22G-RNAs ($\log_2$FC $\geq$ 1, FDR $\leq$ 0.05), blue = downregulated 22G-RNAs
545 ($\log_2$FC $\leq$ -1, FDR $\leq$ 0.05). **c,** Venn diagram showing overlap between the 69 HRDE-1–silenced
546 genes (**Fig. 1b**) and those with significant 22G-RNA changes in G0 and G4 in **b**.
547 **Extended Data Fig. 6: The granule component, ZNFX-1, is required for small RNA**
548 **maintenance but not silencing of HRDE-1-silenced genes. a,** Box plot of $\log_2$ fold change
549 (FC) of 22G-RNAs in *hrde-1*, *znfx-1*, and *znfx-1;hrde-1* compared to wild-type for the 69 genes

550 upregulated in G0 and G4 HRDE-1-depleted L4 larvae (**Fig. 1b**). Data from Ouyang et al.,
551 2022. **b,** Genome browser views of representative targets, F07B7.1 and F15D4.5, showing
552 22G-RNAs for *hrde-1*, *znfx-1*, and *znfx-1;hrde-1* (WT, grey; *hrde-1*, green; *znfx-1*, yellow;
553 double mutant, lime). TE = mapped transposable elements. Data are averaged from two
554 biological replicates (Ouyang et al., 2022). **c,** PolyUGylation assay for HRDE-1–silenced genes
555 that lose 22G-RNAs transgenerationally in wildtype (wt), *hrde-1* and *znfx-1*, backgrounds. The
556 housekeeping gene *gsa-1* is included as a control. **d,** RT–qPCR analysis of HRDE-1–silenced
557 genes from **Fig. 5e** in *znfx-1* (yellow) and wild-type (green) exposed to auxin or control at the
558 L4 stage. Expression values are normalized to *act-3*. Bars represent mean $\log_2$ fold change
559 (FC), dots indicate biological replicates (n = 3-5). **e,** RT–qPCR analysis of selected genes as in
560 **Fig. 5f** in HRDE-1-depleted G0 and G1 worms at the L4 stage in control and *znfx-1* mutant
561 backgrounds, normalized to *act-3*. Bars show mean $\log_2$FC; dots represent biological replicates
562 (n = 4–5).

563 **Extended Data Fig. 7: HRDE-1 silencing maintenance requires 22G-RNA biogenesis. a,**
564 PolyUGylation assay for *bath-13* across control (blue), G0 and G4 depletion (red), and R1, R4,
565 and R6 recovery generations (purple). *gsa-1* serves as control. **b,** RT–qPCR analysis of selected
566 genes as in **Fig. 6f** in G0, R1, and R2 worms at the L4 stage, normalized to *act-3*. Bars show
567 mean $\log_2$FC; dots represent biological replicates (n = 3–5). Bottom: corresponding average
568 fold change of 22G-RNAs for each gene across generations.

569

570 **Methods**

571 Strains and worm culture

572 Worms were grown at 20ºC in NGM plates and fed on OP50 using standars methods[33] . For
573 staged L4 larvae, worms were synchronized by bleaching. Briefly, gravid adults were incubated
574 5 min at 60 RPM in a 0.2 N NaOH and 1.5% NaOCl solution, washed three times, and

575 incubated overnight for hatching with M9 buffer. 40,000 starved L1 larvae were placed on 150
576 mm NGM plates with 1mL of fresh 100X OP50 or NGM supplemented with Ethanol (0.2%
577 v/v) or Auxin (indole-3-acetic-acid, 500 µM in Ethanol) for Auxin-inducible degradation
578 experiments. For transgenerational experiments, L4 larvae were collected at each generation
579 (around 44 hph), while one plate was kept until 72 hph for bleaching gravid adults to obtain
580 the next generation.

581 Generation of CRISPR–Cas9 lines

582 Cas9-guide RNA (gRNA) ribonucleoprotein complexes were microinjected into the
583 hermaphrodite syncytial gonad[34]. AID CRISPR-Cas9 tags were generated using double-
584 stranded DNA repair templates (30bp homology arms on each side) amplified by PCR using
585 an AID::3xFlag gBlock (IDT) sequence. Silent mutations were included where necessary in the
586 repair templates to prevent Cas9 cleavage. Mix concentrations were adapted from a previous
587 study[35]. In brief, 10 µl mixes typically contained the following final concentrations: 0.1µg/µL
588 Cas9-NLS protein (TrueCut V2, Invitrogen), 100 ng/µl in vitro transcribed target-gene gRNA,
589 80ng/µl of target-gene single-stranded DNA (ssDNA) repair template or 300 ng/µl target-gene
590 double-stranded DNA (dsDNA) repair template, and 80 ng/µL pRF4 (roller marker). Cas9 and
591 the target-gene gRNA were pre-incubated for 10-15 minutes at 37°C before adding the other
592 components to the mixture. dsDNA repair templates were subjected to a melting/annealing step
593 before addition to the final mix.

594 Worm population sorting

595 Worms were prepared and collected as described before[6]. Briefly, we obtain large populations
596 of precisely developmentally staged worms for genome-wide approaches, using a COPAS
597 Biosorter (Union Biometrica). For obtaining synchronous L4 population, among 40,000 to
598 80,000 larvae were harvested at 44 hph. To establish the sorting gate, for each sample, ~ 100
599 worms were collected and inspected under a 40X objective brightfield microscope. The number

600 of worms on each substage of the L4 development window was scored according to the vulva
601 shape[36] . Larvae were sorted using a gate enriched for L4.4-4.5 larvae. All conditions of the
602 same biological replicate were collected on the same day. 1,000 worm aliquots were harvested
603 and spun down for 0.5 min at 0.7 g to remove sorting liquid, and flash-frozen in dry ice.

604 RNA fluorescent in situ hybridization (RNA FISH)

605 RNA FISH was performed as described before[6]. For F07B7.1, probes were designed in the
606 exon regions that do not overlap with annotated transposable element sequences. We used
607 unlabeled primary probes and Cy5 fluorescently labeled secondary detector oligonucleotides.
608 Worms were harvested at 44 hph, incubated in fixative solution for 40 min at room temperature,
609 and stored in 70% Ethanol. Fixated larvae were washed once in wash buffer (10% formamide,
610 2× SSC buffer (Ambion)) and hybridized with the corresponding FLAP-containing probes in
611 100 µL hybridization buffer (10% dextran sulfate, 2 mM vanadyl-ribonucleoside complex,
612 0.02% RNAse-free BSA, 50 µg E. coli tRNA, 2× SSC, 10% formamide) at 30 ˚C overnight.
613 Hybridized embryos were washed twice with wash buffer, with DAPI in the second wash for
614 nuclei staining, and once in 2× SSC buffer before imaging. Right before imaging, embryos
615 were resuspended in 100 µL antifade buffer (0.4% glucose, 10 µM Tris-HCl pH 8, 2× SSC)
616 with 1 µL catalase (Sigma-Aldrich) and 1 µL glucose oxidase (3.7 mg/mL, Sigma-Aldrich).
617 Imaging was performed in an Andor BC43 spinning disk confocal microscope, and image
618 processing was done in FIJI[37] .

619 Germline nuclei isolation.

620 260,000 starved L1 larvae were plated in NGM-ethanol (control) or NGM-auxin plates
621 (HRDE-1 or SET-25 germline-depletion) and grown for 44 h for L4 larvae harvesting. Worms
622 were washed out from plates and rinsed three times with 1X M9 buffer by centrifuging for 30
623 seconds at 0.7 g. After the last wash, M9 was removed as much as possible, and the worms
624 were resuspended in 1.5 mL of cold Nuclear Extraction Buffer (NEB)[14] with 1X EDTA-free

625 Protease Inhibitors (Thermo Scientific, 78425). Worms were lysed in a Steel-Dounce diameter
626 XX by applying 65-70 strokes. Worm lysis was monitored by inspection under a stereoscope
627 (Zeiss), and the presence of GFP-positive nuclei was determined by mixing 2 µl of lysate with
628 2 µl of VECTASHIELD® Antifade Mounting Medium with DAPI (Vector Laboratories) and
629 inspection under a Zeiss Axio Imager M2 microscope equipped with a Princeton Instrument
630 PIXIS 926 1024 camera, using Plan-Apochromat 20x/1.40 objectives. Lysate was split into
631 ~300 µl aliquots in six tubes, and 1 mL of NEB was added. The lysate was cleared by 4-minute
632 centrifugation at 100 g and 4°C. Approximately 800-1,000 µl of supernatant were transferred
633 to a new tube and centrifuged for 4 minutes at 1,000 g and 4 °C to pellet the nuclei. Supernatant
634 was discarded, and the pellet was resuspended in ~ 100 µl of the remaining NEB buffer and
635 pooled into two tubes. Nuclei were pelleted by 4-minute centrifugation at 1,000 g and 4ºC,
636 resuspended in NEB without glycerol and 1X EDTA-free Protease Inhibitors, and kept on ice
637 until sorting.

638 Germline nuclei sorting.

639 Nuclei suspension was filtered and diluted 1:3-1:5 in cold NEB without glycerol and 1X
640 EDTA-free Protease Inhibitors (Thermo Scientific™, 78425). Nuclei were analyzed and sorted
641 using an Aria FACS III system (BD Biosciences). Aliquots of 500,000 GFP-positive nuclei
642 were collected in 1.5 mL tubes with 100 µl of NEB without glycerol and 1X EDTA-free
643 Protease Inhibitors and kept on ice. After sorting, four to six aliquots were centrifuged for 4
644 minutes at 1,100 g and 4ºC, the supernatant was discarded, leaving ~50-100 µl to not perturb
645 the nuclei pellet (not visible). Nuclei were gently resuspended avoiding the formation of
646 bubbles and pooled into one tube. Nuclei were pellet by centrifuging for 4 minutes at 1,100 g
647 and 4ºC, the supernatant was discarded, and nuclei were resuspended in 100 µl of NEB with
648 glycerol and 1X EDTA-free Protease Inhibitors per initial 500,000 nuclei and stored at -20ºC
649 until further processing.

650 For RNA extraction, nuclei were resuspended in 50 µl per 500,000 initial nuclei, and 1 mL of
651 TriZol was added before freezing.
652 For GRO-seq, nuclei were resuspended in 30 µL of GRO-seq Nuclear freezing buffer[14] and
653 nuclear run-on was performed immediately, as described below.
654 Western Blot
655 Western blots were performed to monitor AID:Flag:HRDE-1 levels and its depletion upon
656 auxin exposure; control worms were collected in parallel. For sorted larvae, 1,000 worms were
657 resuspended in 50 µl of 4X NuPage LDS and 1X NuPage Reducing agent (Thermo
658 Scientific™). For larvae used for nuclei preparation, 5 to 10 µl of packed worms were taken
659 before extraction and mixed with 100 µl of 4X LDS and 1X Reducing agent. Worms were lysed
660 by 10 minutes incubation at 95ºC. Then centrifuged for 10 minutes at 20ºC and 12000 g, ~30-
661 50% of sample was used for SDS-PAGE electrophoresis in 4-12% NuPage polyacrylamide
662 gels. Gels were run 50 min at 180V in 1X MOPS buffer (Thermo Scientific™), and transfer to
663 Nylon membrane by wet transfer in 1X NuPage wet transfer with 10% Methanol at 4ºC for 2.5
664 hours at 30 V. Transfers were monitored with Ponceau staining, and unstained before blocking
665 with 5% blocking reagent for 30 min at room temperature. After the membranes were rinsed
666 twice with 1X PBS and 0.1% Tween 20, all incubations were performed in the same buffer.
667 Primary antibody incubation was performed overnight at 4 °C with agitation. After, membranes
668 were washed four times before secondary antibody incubation for 2 hours at room temperature
669 and agitation. Antibody dilutions used: mouse anti-Flag 1:5000 (Sigma, F1804), mouse anti-
670 GADPH (Abcam, AB125247) 1:2000 and the secondary antibodies used were goat anti-mouse
671 Alexa Fluor 488 (Invitrogen, A11001) and goat anti-rabbit Alexa Fluor 568 (Invitrogen
672 A11011) antibodies at a dilution of 1:10000.
673 RNA extraction.

674 1 mL of TriZol reagent (Invitrogen) was used following the manufacturer's instructions. When
675 extracting RNA from whole worms, 1000-2000 L4 sorted larvae or 10 µl of L4 (44 hph) packed
676 worms were mixed with TriZol, and subjected to four to five cycles of freeze-thaw in dry ice
677 and 2 minutes of agitation at 25ºC and 2000 rpm in a Thermomixer (Eppendorf). Then, 100 µl
678 of 1-Bromo-3-chloropropane (Sigma, B9673) was added and vortexed. After 15 minutes of
679 incubation at room temperature, samples were centrifuged for 15 minutes at 12000 g and 4ºC,
680 and the aqueous phase was transferred to a new tube. 2 µl of glycoblue (Invitrogen, AM9515)
681 and 1 volume of Isopropanol (Sigma) were added and vortexed to mix. Samples were incubated
682 at room temperature for 15 min and RNA was precipitated by centrifuging 15 min at 12000 g
683 and 4ºC. Pellet was washed twice in 75% Ethanol and centrifuging 5 minutes at 7500 g and
684 4ºC, pellet was resuspended in nuclease-free water. Concentration and quality were estimated
685 using Nanodrop (Thermo Scientific™).

686 RT-qPCR.

687 Reverse transcription was performed using M-MLV reverse transcriptase (Invitrogen), and
688 qPCR was performed using Applied Biosystems PowerUp SYBR Green PCR Master mix and
689 using QuantStudio 3 Real-Time PCR System (Applied Biosystems).

690 Total RNA library preparation.

691 Total RNA was extracted as detailed above. RNA was treated with 1 unit of Turbo DNAse
692 (Invitrogen, AM2238) for 30 min at 37ºC and immediately purified using 1.8X ArgentCourt
693 RNA purification beads and 3X Isopropanol. This step was skipped for RNA extracted from
694 isolated germline nuclei. RNA integrity number was assessed with Agilent Tapestation 2200
695 and used to determine the fragmentation time during library preparation. 100 ng of total RNA
696 from whole worm or RNA from 500,000 germline nuclei were subjected to ribosomal RNA
697 depletion using DNA probed and DNAse H as described before[16]. DNA probes were degraded

698 by Turbo DNAse treatment and bead purification as explained before. Strand-specific libraries
699 were prepared with NEBNext® Ultra™ II Directional RNA Library Prep Kit (E7770).
700 Small RNA library preparation.
701 Libraries were prepared as described before[16]. Briefly, around 5 µg of total RNA was mixed
702 1:1 volume with 2X Novex® TBE-Urea Sample Buffer, denatured for 3 min at 95ºC, and kept
703 on ice until gel loading. RNAs were size separated in 15% NuPage 7% Urea polyacrylamide
704 gels (Invitrogen) in 1X TBE buffer for 45 min at 180V. The RNA cut and extracted from gel
705 was precipitated with 2 µL of Glycoblue (Invitrogen, AM9515) and 3 volumes of 100%
706 Ethanol. After incubation on ice, the samples were centrifuged and washed once with 75%
707 ethanol. Isolated small RNAs were treated with 5' Polyphosphatase, ligated with 3' and 5' end
708 adaptors, and amplified by PCR using Illumina indexed primers. PCRs were purified with
709 ArgentCourt DNA beads and analyzed using Tapestation. Libraries were pooled and size
710 selected using Pippinprep. Libraries were purified again using ArgentCourt beads and
711 quantified using Qubit to estimate molarity, based on a library size of 148 bp. An equimolar
712 proportion of each library was mixed for sequencing.
713 GRO-seq library preparation.
714 GRO-seq was performed as previously described[14] . Briefly, nuclear Run-On reactions were
715 performed by incorporating 1 mM Bio-11UTP, followed by RNA extraction with Trizol and
716 RNA fragmentation. Biotinylated nascent RNA was then purified using DynabeadTM
717 MyOneTM Streptavidin C1 (Cat#65001). To prepare libraries, purified RNAs were first treated
718 with T4 Polynucleotide Kinase (New England Biolabs) to repair the 5'-OH ends. This was
719 followed by 3' and 5' adaptor ligation. Adaptor-ligated RNAs were then reverse transcribed
720 using SuperScript IV Reverse Transcriptase (Thermo Fisher Scientific), following the
721 manufacturer's protocol with slight modifications: the reaction was incubated for 1 hour at
722 50°C and 10 minutes at 80°C. cDNA was PCR amplified using specific primers and the

723 NEBNext Ultra II Q5 Master Mix 2x (New England Biolabs) for 15 cycles. Libraries were
724 analyzed using the Agilent 2200 TapeStation System with high sensitivity D1000 screentapes
725 and quantified with the Qubit Fluorometer High Sensitivity dsDNA assay kit (Thermo Fisher
726 Scientific, Q32851). The multiplexed libraries were then sequenced on the Illumina NextSeq
727 2000 platform.

728 CUT&Tag library preparation

729 Cut&Tag was performed following the EpiCypher protocol with few modifications. Briefly.
730 100 µL of the nuclei resuspension generated as described above was used for binding to
731 Concanavalin A beads (Epicypher 21-1401). Bead-bound nuclei were resuspended in 100 µL
732 of Antibody150 buffer (20 mM HEPES pH 7.5, 150 mM NaCl, 0.01% digitonin, 2 mM EDTA,
733 protease inhibitors, 0.5 mM spermidine), and 1 µg of primary antibody was added. Reactions
734 were incubated overnight in a thermocycler shaker set up at 4°C with shaking cycles at 2000
735 rpm, 15 seconds ON 45 seconds OFF. 1 µg of secondary antibody was added, followed by
736 tagmentation with Tn5 (Epicypher 15-1117). Resulting libraries were amplified with i5 and i7
737 primers using 13 to 15 PCR cycles and purified using AMPure beads. Libraries were analyzed
738 using the Agilent 2200 TapeStation System with high-sensitivity D1000 screentapes and
739 quantified with the Qubit Fluorometer High Sensitivity dsDNA assay kit (Thermo Fisher
740 Scientific, Q32851). Four biological replicates were performed for each experiment.

741 Library sequencing.

742 All library preparations were compatible for Illumina sequencing using NextSeq2000
743 sequencers and conventional or XLEAP-SBS technology, P1 or P2 100 cycles NextSeq2000
744 reagents.

745 Sequencing data analysis

746 All the sequencing data were demultiplexed with Illumina bcl2fastq converter (version
747 v2.17.1.14), and quality control was performed with fastQC (version v0.11.5).

RNA-seq analysis

HISAT2 version 2.0.4[38] was used for mapping RNA-seq reads aligned to the *C. elegans* genome sequence (ce11, *C. elegans* Sequencing Consortium WBcel235). After alignment, reads mapping to annotated protein-coding genes were counted using featureCounts (version 2.0.1)[39]. Counted reads for protein-coding genes were used for differential expression analysis using the R/Bioconductor package DESeq2 (version 1.26.0)[40].

Small RNA-seq analysis

The analysis of small RNA sequencing was performed as previously described[16].

GRO-seq analysis

Analysis of the sequencing data was performed as previously described[43] . The scripts and workflows are available at https://gitlab.pasteur.fr/bli/bioinfo_utils.

CUT and Tag

Reads were aligned with Bowtie242 to the WBcel235 genome, with the following options: "--local --very-sensitive-local --dovetail --soft-clipped-unmapped-tlen". Reads were additionally deduplicated using samtools and filtered to keep those with a single discovered alignment. Peaks were called using MACS2 with the following parameters: "callpeak -q 0.05 -g ce --keep-dup all". Peaks were further filtered to keep those with MACS2 FDR < 0.01 in merged reads from all conditions, and FDR < 0.05 in at least two individual replicates. Quantifications for the selected set of peaks were done for each dataset using Subread featureCounts and analyzed using a DESeq2 generalized linear model.

Statistics and reproducibility

All the experiments shown in this study were performed independently at least twice, and the exact number of biological replicates is indicated on each figure legend.

Data and code availability

All the sequencing data are available upon request.

Acknowledgments

We would like to thank all the members of the Cecere laboratory for the helpful discussions on the manuscript and suggestions on the project. We thank Dr. Florian Muller, head of the Photonic BioImaging platform, and Dr. Gaëlle Letort, research engineer in the Department of Developmental and Stem Cell Biology, for their assistance on RNA FISH imaging

interpretation. We thank the Caenorhabditis Genetics Center (CGC) for *C. elegans* strains, supported by the National Institutes of Health - Office of Research Infrastructure Programs (P40 OD010440). We thank Carolyn Phillips for sharing rde-8 and nyn-1:nyn-2 strains. We thank the Flow Cytometry, Photonic BioImaging, and Biomics facilities at Institut Pasteur. This project has received funding from the Institut Pasteur, the CNRS, and the European Union's Horizon 2020 research and innovation program (grant agreement no. 101002999). A.M.L.R. received funding from the European Union under the HORIZON-MSCA-2022-PF-01 program no. 101109836 — MOMENTS and A.K.M. received funding from LabEx Revive fellowship ANR-10-LBX-73.

Author contributions

A.M.L.R and G.C. identified and developed the core questions of the work and supervised the whole project, contributed to the data analysis, and wrote the manuscript. A.K.M. developed the germline nuclei isolation protocol, and together with J.J. and A.M.L.R., adapted it for downstream genomic approaches (total RNA-seq, CUT&Tag, and GRO-seq). P.Q. and A.M.L.R. performed antibody screenings for the CUT&Tag protocol. A.C. developed pipelines for small RNA-seq, RNA-seq, and CUT&Tag analysis, and assisted A.M.L.R. in downstream data examination. A.M.L.R. and J.J. performed CUT&Tag experiments. A.M.L.R. performed RNA, small RNA, GRO-seq, and RNA FISH experiments. L.B. performed together with O.F. the RNAi inheritance assay. A.M.L.R. and S.I. performed the polyUGylation assays. A.M.L.R. and S.C. performed RT-qPCR of AID and mutant strains. L.B. assisted A.M.L.R. with the COPAS operation for staged-worm sorting. L.B. and J.O. generated all the strains and crosses used in this project and helped with worm growing and maintenance.

Competing interests

The authors declare no competing interests.

Materials & Correspondence

Correspondence and material requests should be addressed to Germano Cecere:

germano.cecere@pasteur.fr

References

1. Heard, E. & Martienssen, R. A. Transgenerational Epigenetic Inheritance: Myths and Mechanisms. *Cell* **157**, 95–109 (2014).

2. Skvortsova, K., Iovino, N. & Bogdanović, O. Functions and mechanisms of epigenetic inheritance in animals. *Nat Rev Mol Cell Bio* **19**, 774–790 (2018).

3. Cecere, G. Small RNAs in epigenetic inheritance: from mechanisms to trait transmission. *Febs Lett* **595**, 2953–2977 (2021).

4. Buckley, B. A. *et al.* A nuclear Argonaute promotes multigenerational epigenetic inheritance and germline immortality. *Nature* **489**, 447–451 (2012).

5. de Albuquerque, B. F. M., Placentino, M. & Ketting, R. F. Maternal piRNAs Are Essential for Germline Development following De Novo Establishment of Endo-siRNAs in Caenorhabditis elegans. *Dev Cell* **34**, 448–456 (2015).

6. Cornes, E. *et al.* piRNAs initiate transcriptional silencing of spermatogenic genes during C. elegans germline development. *Dev Cell* **57**, 180-196.e7 (2022).

7. Schwartz-Orbach, L. *et al.* Caenorhabditis elegans nuclear RNAi factor SET-32 deposits the transgenerational histone modification, H3K23me3. *Elife* **9**, e54309 (2020).

8. Gu, S. G. *et al.* Amplification of siRNA in Caenorhabditis elegans generates a transgenerational sequence-targeted histone H3 lysine 9 methylation footprint. *Nat Genet* **44**, 157–164 (2012).

9. Kalinava, N., Ni, J. Z., Peterman, K., Chen, E. & Gu, S. G. Decoupling the downstream effects of germline nuclear RNAi reveals that H3K9me3 is dispensable for heritable RNAi and the maintenance of endogenous siRNA-mediated transcriptional silencing in Caenorhabditis elegans. *Epigenetics Chromatin* **10**, 6 (2017).

10. Ouyang, J. P. T., Zhang, W. L. & Seydoux, G. The conserved helicase ZNFX-1 memorializes silenced RNAs in perinuclear condensates. *Nat. Cell Biol.* **24**, 1129–1140 (2022).

11. Rieger, I. *et al.* Nucleus-independent transgenerational small RNA inheritance in Caenorhabditis elegans. *Sci. Adv.* **9**, eadj8618 (2023).

12. Kalinava, N. *et al.* C. elegans Heterochromatin Factor SET-32 Plays an Essential Role in Transgenerational Establishment of Nuclear RNAi-Mediated Epigenetic Silencing. *Cell Rep.* **25**, 2273-2284.e3 (2018).

13. Kaya-Okur, H. S. *et al.* CUT&Tag for efficient epigenomic profiling of small samples and single cells. *Nat. Commun.* **10**, 1930 (2019).

845 14. Quarato, P. & Cecere, G. Global Run-On sequencing to measure nascent transcription in
846 C. elegans. *Star Protoc* **2**, 100991 (2021).

847 15. Zhang, L., Ward, J. D., Cheng, Z. & Dernburg, A. F. The auxin-inducible degradation
848 (AID) system enables versatile conditional protein depletion in C. elegans. *Dev. (Camb.,*
849 *Engl.)* **142**, 4374–4384 (2015).

850 16. Barucci, G. *et al.* Small-RNA-mediated transgenerational silencing of histone genes
851 impairs fertility in piRNA mutants. *Nat. Cell Biol.* **22**, 235–245 (2020).

852 17. Guang, S. *et al.* An Argonaute Transports siRNAs from the Cytoplasm to the Nucleus.
853 *Science* **321**, 537–541 (2008).

854 18. Tsanov, N. *et al.* smiFISH and FISH-quant – a flexible single RNA detection approach
855 with super-resolution capability. *Nucleic Acids Res.* **44**, e165–e165 (2016).

856 19. Chen, S. & Phillips, C. M. HRDE-2 drives small RNA specificity for the nuclear
857 Argonaute protein HRDE-1. *Nat. Commun.* **15**, 957 (2024).

858 20. Towbin, B. D. *et al.* Step-Wise Methylation of Histone H3K9 Positions Heterochromatin
859 at the Nuclear Periphery. *Cell* **150**, 934–947 (2012).

860 21. Greer, E. L. *et al.* A Histone Methylation Network Regulates Transgenerational
861 Epigenetic Memory in C. elegans. *Cell Rep.* **7**, 113–126 (2014).

862 22. Ding, Y.-H., Ochoa, H. J., Ishidate, T., Shirayama, M. & Mello, C. C. The nuclear
863 Argonaute HRDE-1 directs target gene re-localization and shuttles to nuage to promote small
864 RNA-mediated inherited silencing. *Cell Rep.* **42**, 112408 (2023).

865 23. Shukla, A. *et al.* poly(UG)-tailed RNAs in genome protection and epigenetic inheritance.
866 *Nature* **582**, 283–288 (2020).

867 24. Tsai, H.-Y. *et al.* A Ribonuclease Coordinates siRNA Amplification and mRNA
868 Cleavage during RNAi. *Cell* **160**, 407–419 (2015).

869 25. Phillips, C. M., Montgomery, T. A., Breen, P. C. & Ruvkun, G. MUT-16 promotes
870 formation of perinuclear Mutator foci required for RNA silencing in the C. elegans germline.
871 *Gene Dev* **26**, 1433–1444 (2012).

872 26. Wan, G. *et al.* Spatiotemporal regulation of liquid-like condensates in epigenetic
873 inheritance. *Nature* **557**, 679–683 (2018).

874 27. Ashe, A. *et al.* piRNAs Can Trigger a Multigenerational Epigenetic Memory in the
875 Germline of C. elegans. *Cell* **150**, 88–99 (2012).

876 28. Akay, A. *et al.* The Helicase Aquarius/EMB-4 Is Required to Overcome Intronic Barriers
877 to Allow Nuclear RNAi Pathways to Heritably Silence Transcription. *Dev Cell* **42**, 241-
878 255.e6 (2017).

879 29. Guang, S. *et al.* Small regulatory RNAs inhibit RNA polymerase II during the elongation
880 phase of transcription. *Nature* **465**, 1097–1101 (2010).

881 30. Shukla, A., Perales, R. & Kennedy, S. piRNAs coordinate poly(UG) tailing to prevent
882 aberrant and perpetual gene silencing. *Curr Biol* (2021) doi:10.1016/j.cub.2021.07.076.

883 31. Duempelmann, L. *et al.* Inheritance of a Phenotypically Neutral Epimutation Evokes
884 Gene Silencing in Later Generations. *Mol Cell* **74**, 534-541.e4 (2019).

885 32. Andersen, P. R., Tirian, L., Vunjak, M. & Brennecke, J. A heterochromatin-dependent
886 transcription machinery drives piRNA expression. *Nature* **549**, 54–59 (2017).

887 33. Stiernagle, T. Maintenance of C. elegans. *WormBook : online Rev. C elegans Biol.* 1–11
888 (2006) doi:10.1895/wormbook.1.101.1.

889 34. Paix, A., Folkmann, A., Rasoloson, D. & Seydoux, G. High Efficiency, Homology-
890 Directed Genome Editing in Caenorhabditis elegans Using CRISPR-Cas9 Ribonucleoprotein
891 Complexes. *Genetics* **201**, 47–54 (2015).

892 35. Dokshin, G. A., Ghanta, K. S., Piscopo, K. M. & Mello, C. C. Robust Genome Editing
893 with Short Single-Stranded and Long, Partially Single-Stranded DNA Donors in
894 Caenorhabditis elegans. *Genetics* **210**, 781–787 (2018).

895 36. Mok, D. Z. L., Sternberg, P. W. & Inoue, T. Morphologically defined sub-stages of C.
896 elegans vulval development in the fourth larval stage. *BMC Dev. Biol.* **15**, 26 (2015).

897 37. Schindelin, J. *et al.* Fiji: an open-source platform for biological-image analysis. *Nat.*
898 *Methods* **9**, 676–682 (2012).

899 38. Kim, D., Langmead, B. & Salzberg, S. L. HISAT: a fast spliced aligner with low memory
900 requirements. *Nat. Methods* **12**, 357–360 (2015).

901 39. Liao, Y., Smyth, G. K. & Shi, W. featureCounts: An efficient general-purpose program
902 for assigning sequence reads to genomic features. *arXiv* (2013)
903 doi:10.48550/arxiv.1305.3347.

904 40. Love, M. I., Huber, W. & Anders, S. Moderated estimation of fold change and dispersion
905 for RNA-seq data with DESeq2. *Genome Biol.* **15**, 550 (2014).

906 41. Ritchie, M. E. *et al.* limma powers differential expression analyses for RNA-sequencing
907 and microarray studies. *Nucleic Acids Res.* **43**, e47–e47 (2015).

908 42. Law, C. W., Chen, Y., Shi, W. & Smyth, G. K. voom: precision weights unlock linear
909 model analysis tools for RNA-seq read counts. *Genome Biol.* **15**, R29–R29 (2014).

910 43. Quarato, P. *et al.* Germline inherited small RNAs facilitate the clearance of untranslated
911 maternal mRNAs in C. elegans embryos. *Nat Commun* **12**, 1441 (2021).

912

Figures

Figure 1

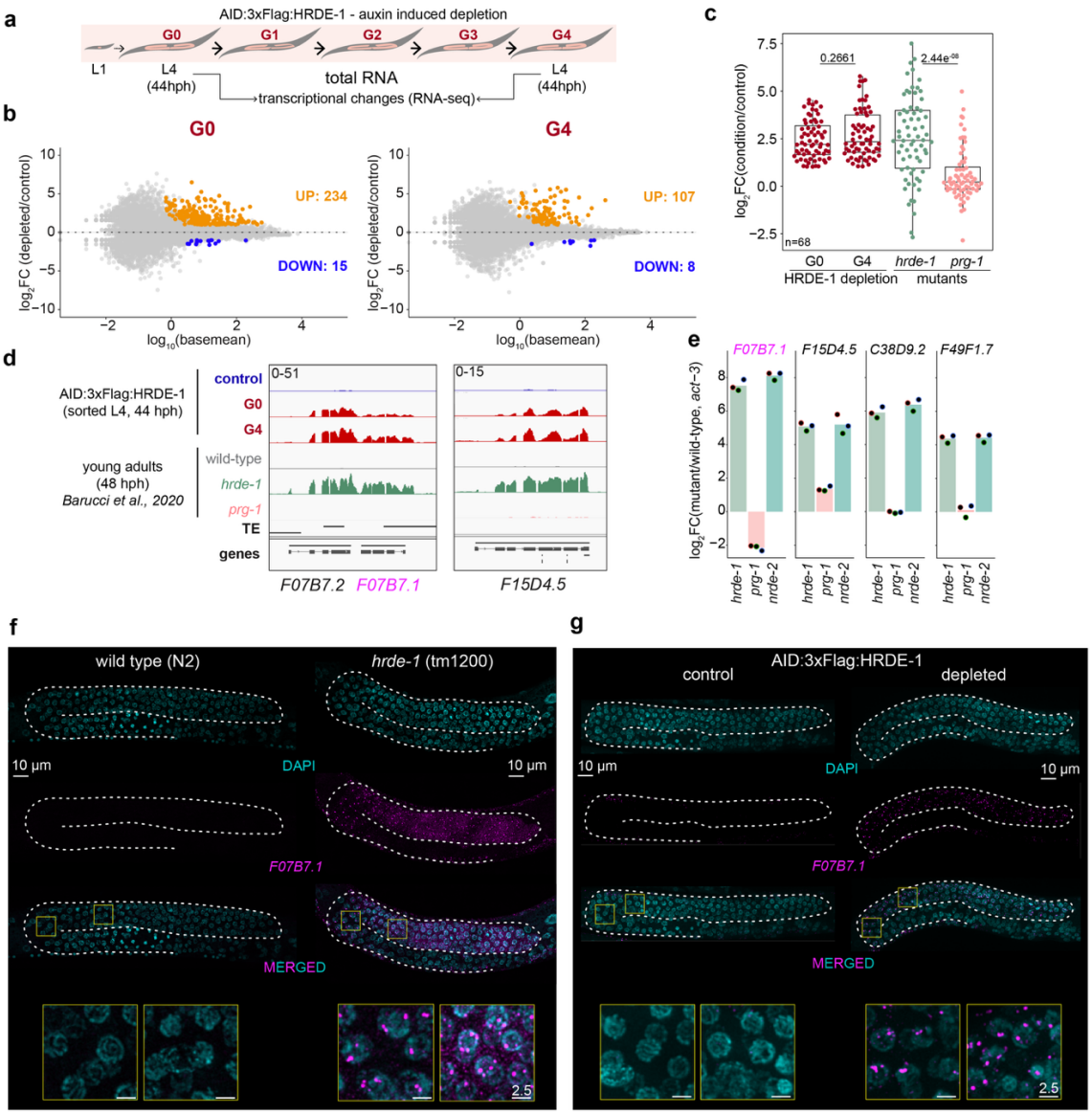

Figure 2

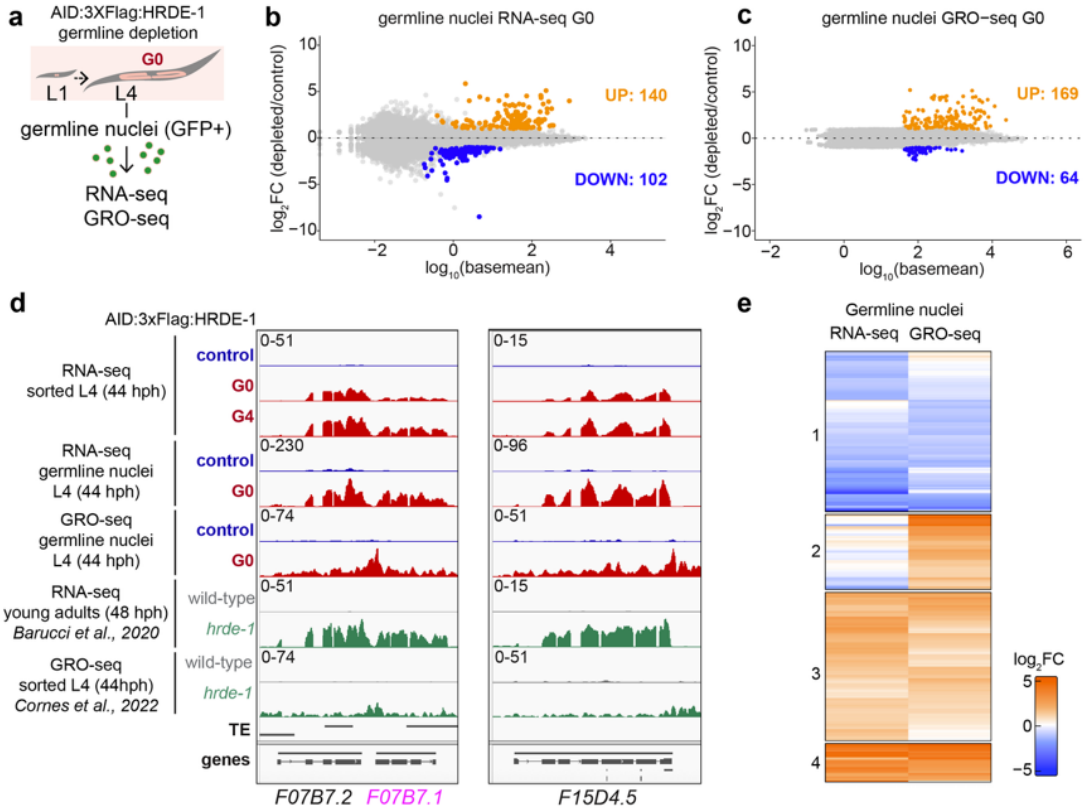
a
AID:3XFlag:HRDE-1
germline depletion
G0
L1
L4
germline nuclei (GFP+)
RNA-seq
GRO-seq
b
germline nuclei RNA-seq G0
UP: 140
DOWN: 102
log2FC (depleted/control)
log10(basemean)
c
germline nuclei GRO−seq G0
UP: 169
DOWN: 64
log2FC (depleted/control)
log10(basemean)
d
AID:3xFlag:HRDE-1
RNA-seq
sorted L4 (44 hph)
control
G0
G4
RNA-seq
germline nuclei
L4 (44 hph)
control
G0
GRO-seq
germline nuclei
L4 (44 hph)
control
G0
RNA-seq
young adults (48 hph)
Barucci et al., 2020
wild-type
hrde-1
GRO-seq
sorted L4 (44hph)
Cornes et al., 2022
wild-type
hrde-1
TE
genes
0-51
0-230
0-74
0-51
0-74
0-15
0-96
0-51
0-15
0-51
F07B7.2
F07B7.1
F15D4.5
e
Germline nuclei
RNA-seq GRO-seq
1
2
3
4
log2FC

Figure 3

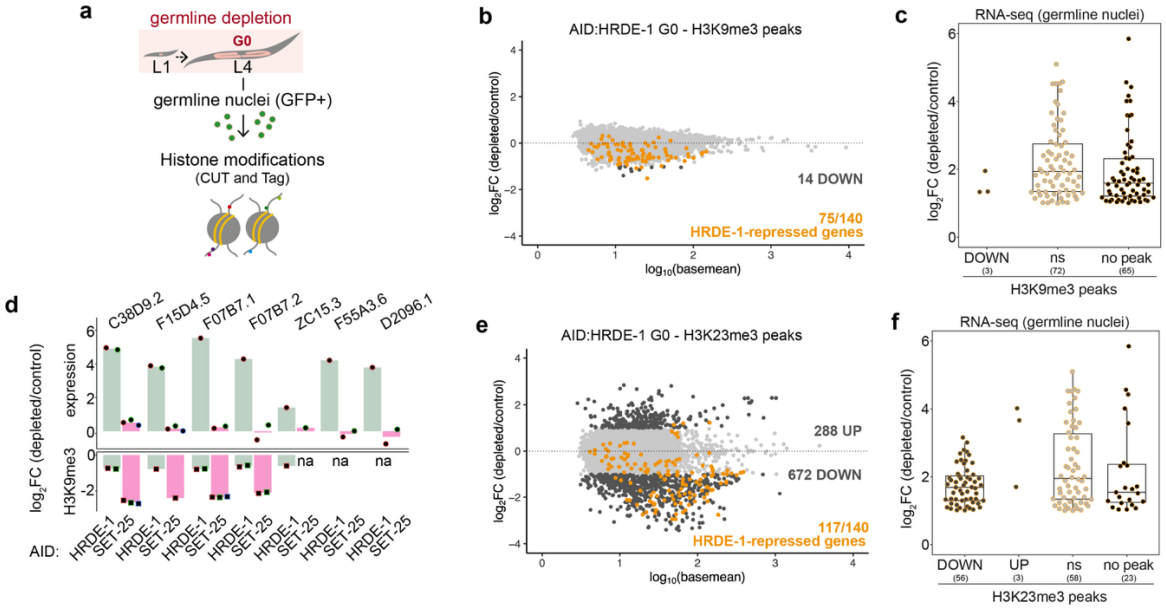
a
germline depletion
G0
L1
L4
germline nuclei (GFP+)
Histone modifications
(CUT and Tag)
b
AID:HRDE-1 G0 - H3K9me3 peaks
14 DOWN
75/140
HRDE-1-repressed genes
log2FC (depleted/control)
log10(basemean)
c
RNA-seq (germline nuclei)
log2FC (depleted/control)
DOWN
ns
no peak
H3K9me3 peaks
d
C38D9.2
F15D4.5
F07B7.1
F07B7.2
ZC15.3
F55A3.6
D2096.1
log2FC (depleted/control)
expression
H3K9me3
na
AID:
HRDE-1
SET-25
e
AID:HRDE-1 G0 - H3K23me3 peaks
288 UP
672 DOWN
117/140
HRDE-1-repressed genes
log2FC (depleted/control)
log10(basemean)
f
RNA-seq (germline nuclei)
log2FC (depleted/control)
DOWN
UP
ns
no peak
H3K23me3 peaks

Figure 4

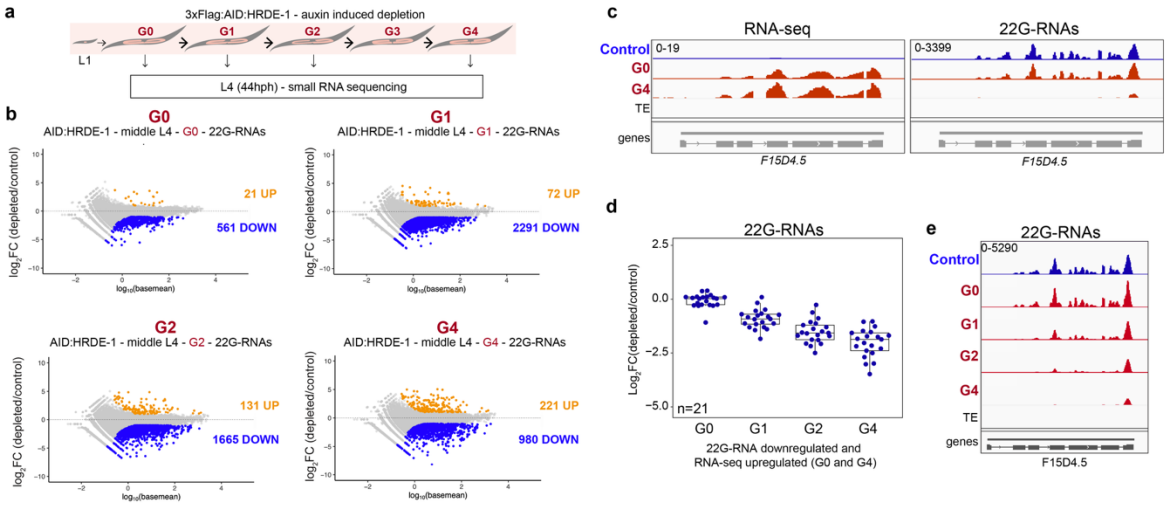
a
3xFlag:AID:HRDE-1 - auxin induced depletion
L1
G0
G1
G2
G3
G4
L4 (44hph) - small RNA sequencing
b
G0
AID:HRDE-1 - middle L4 - G0 - 22G-RNAs
21 UP
561 DOWN
G1
AID:HRDE-1 - middle L4 - G1 - 22G-RNAs
72 UP
2291 DOWN
G2
AID:HRDE-1 - middle L4 - G2 - 22G-RNAs
131 UP
1665 DOWN
G4
AID:HRDE-1 - middle L4 - G4 - 22G-RNAs
221 UP
980 DOWN
log2FC (depleted/control)
log10(basemean)
c
RNA-seq
22G-RNAs
Control
G0
G4
TE
genes
0-19
0-3399
F15D4.5
d
22G-RNAs
Log2FC(depleted/control)
n=21
G0
G1
G2
G4
22G-RNA downregulated and
RNA-seq upregulated (G0 and G4)
e
22G-RNAs
0-5290
Control
G0
G1
G2
G4
TE
genes
F15D4.5

Figure 5

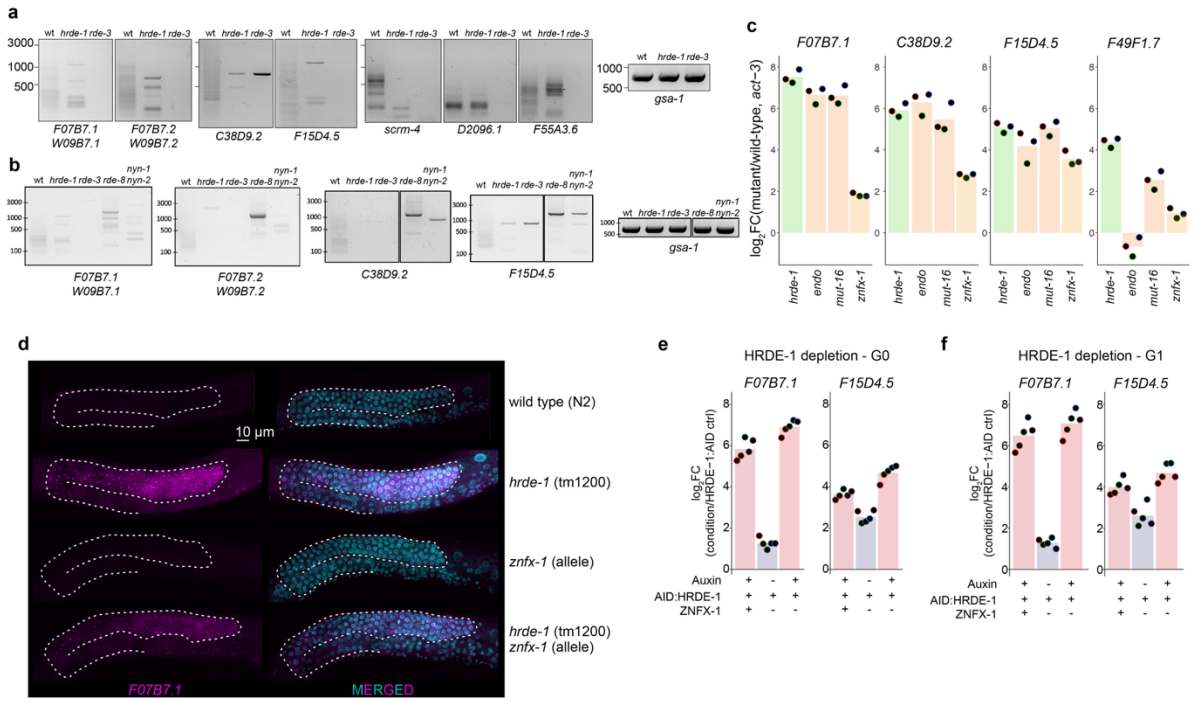
a
wt hrde-1 rde-3
F07B7.1 W09B7.1
F07B7.2 W09B7.2
C38D9.2
F15D4.5
scrm-4
D2096.1
F55A3.6
gsa-1
b
nyn-1
rde-8
F07B7.1 W09B7.1
F07B7.2 W09B7.2
C38D9.2
F15D4.5
gsa-1
c
F07B7.1
C38D9.2
F15D4.5
F49F1.7
log2FC(mutant/wild-type, act-3)
hrde-1
endo
mut-16
znfx-1
d
10 µm
wild type (N2)
hrde-1 (tm1200)
znfx-1 (allele)
hrde-1 (tm1200)
znfx-1 (allele)
F07B7.1
MERGED
e
HRDE-1 depletion - G0
F07B7.1
F15D4.5
log2FC (condition/HRDE-1:AID ctrl)
Auxin
AID:HRDE-1
ZNFX-1
f
HRDE-1 depletion - G1
F07B7.1
F15D4.5
log2FC (condition/HRDE-1:AID ctrl)
Auxin
AID:HRDE-1
ZNFX-1

Figure 6

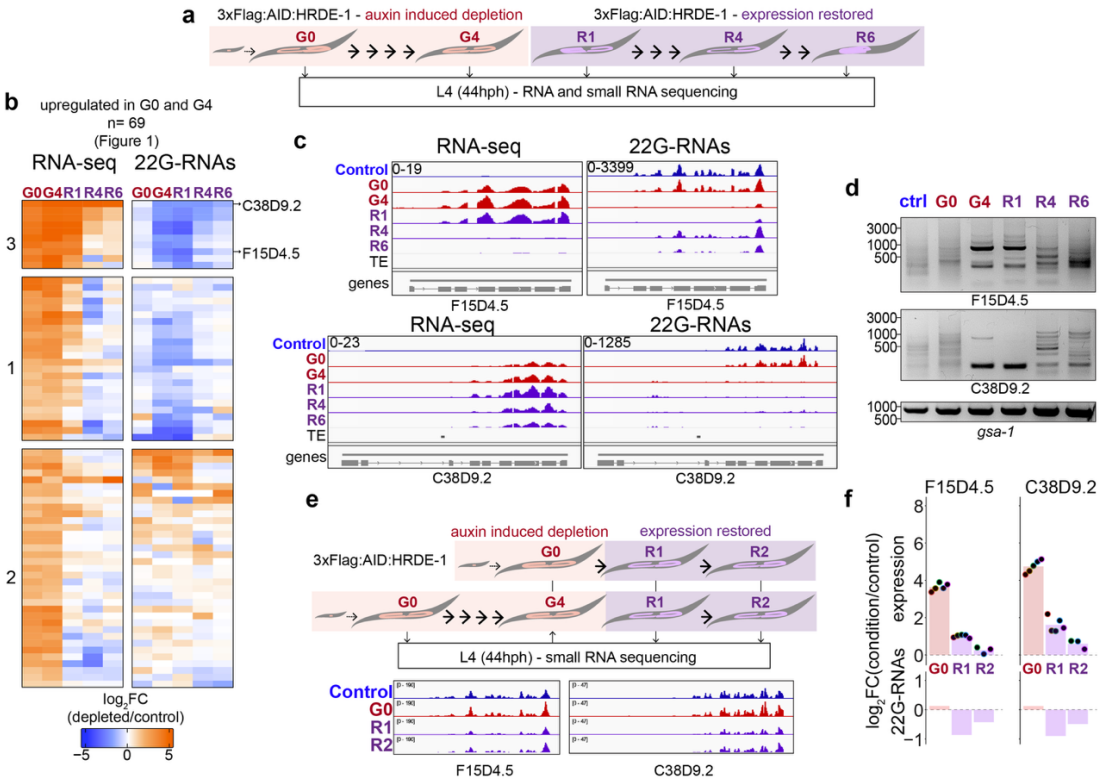
a
3xFlag:AID:HRDE-1 - auxin induced depletion
3xFlag:AID:HRDE-1 - expression restored
G0
G4
R1
R4
R6
L4 (44hph) - RNA and small RNA sequencing
b
upregulated in G0 and G4
n= 69
(Figure 1)
RNA-seq
22G-RNAs
G0G4R1R4R6
C38D9.2
F15D4.5
log2FC
(depleted/control)
c
RNA-seq
22G-RNAs
Control
TE
genes
0-19
0-3399
0-23
0-1285
d
ctrl
gsa-1
e
auxin induced depletion
expression restored
3xFlag:AID:HRDE-1
R2
L4 (44hph) - small RNA sequencing
f
expression
22G-RNAs
log2FC(condition/control)

Extended Data Figures.

Ext. Data Figure 1

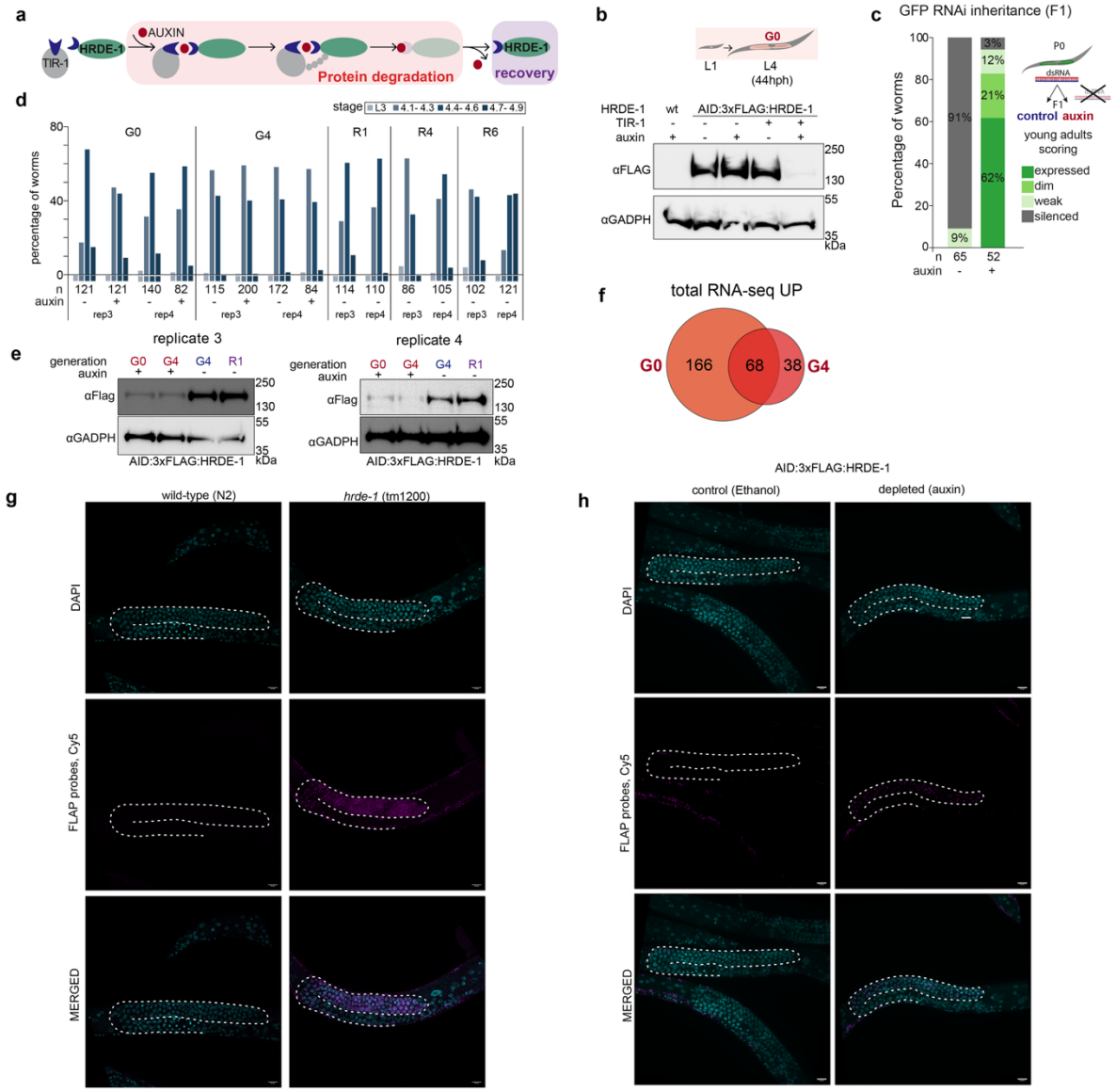

Ext. Data Figure 2

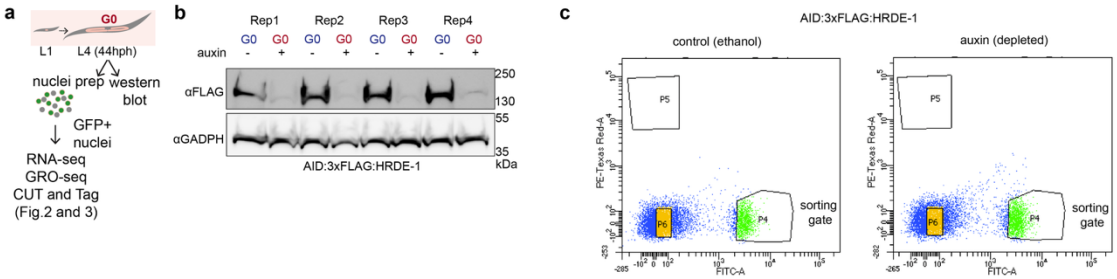

Ext. Data Figure 3

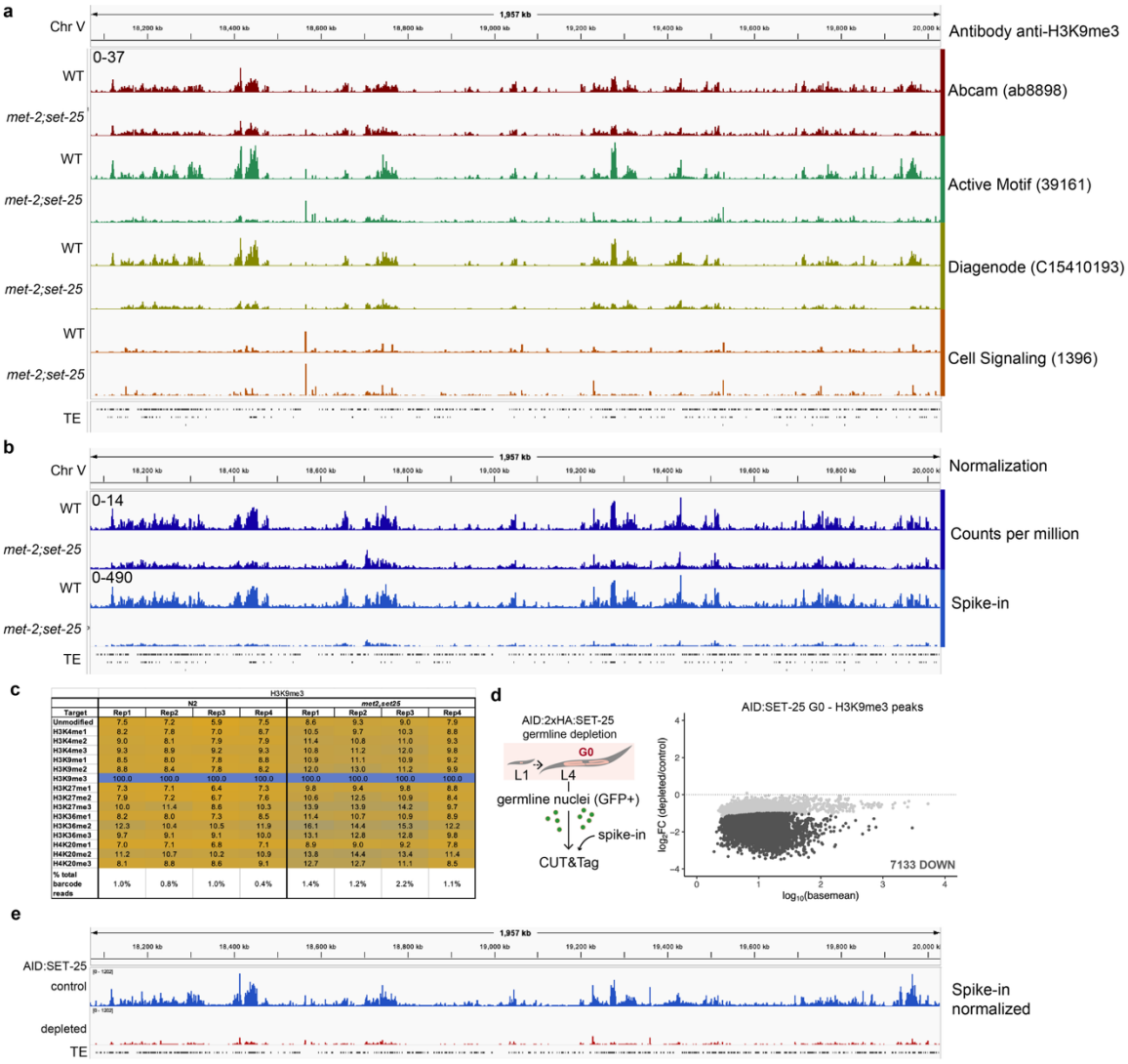

	H3K9me3							
	N2				met2,set25			
Target	Rep1	Rep2	Rep3	Rep4	Rep1	Rep2	Rep3	Rep4
Unmodified	7.5	7.2	5.9	7.5	8.6	9.3	9.0	7.9
H3K4me1	8.2	7.8	7.0	8.7	10.5	9.7	10.3	8.8
H3K4me2	9.0	8.1	7.9	7.9	11.4	10.8	11.0	9.3
H3K4me3	9.3	8.9	9.2	9.3	10.8	11.2	12.0	9.8
H3K9me1	8.5	8.0	7.8	8.6	10.9	11.1	10.9	9.2
H3K9me2	8.8	8.4	7.8	8.2	12.0	13.0	11.2	9.9
H3K9me3	100.0	100.0	100.0	100.0	100.0	100.0	100.0	100.0
H3K27me1	7.3	7.1	6.4	7.3	9.6	9.4	9.8	8.8
H3K27me2	7.9	7.2	6.7	7.6	10.6	12.5	10.9	8.4
H3K27me3	10.0	11.4	8.6	10.3	13.9	13.9	14.2	9.7
H3K36me1	8.2	8.0	7.3	8.5	11.4	10.7	10.9	8.9
H3K36me2	12.3	10.4	10.5	11.9	16.1	14.4	15.3	12.2
H3K36me3	9.7	9.1	9.1	10.0	13.1	12.8	12.8	9.8
H4K20me1	7.0	7.1	6.8	7.1	8.9	9.0	9.2	7.8
H4K20me2	11.2	10.7	10.2	10.9	13.8	14.4	13.4	11.4
H4K20me3	8.1	8.8	8.6	9.1	12.7	12.7	11.1	8.5
% total barcode reads	1.0%	0.8%	1.0%	0.4%	1.4%	1.2%	2.2%	1.1%

Ext. Data Figure 4

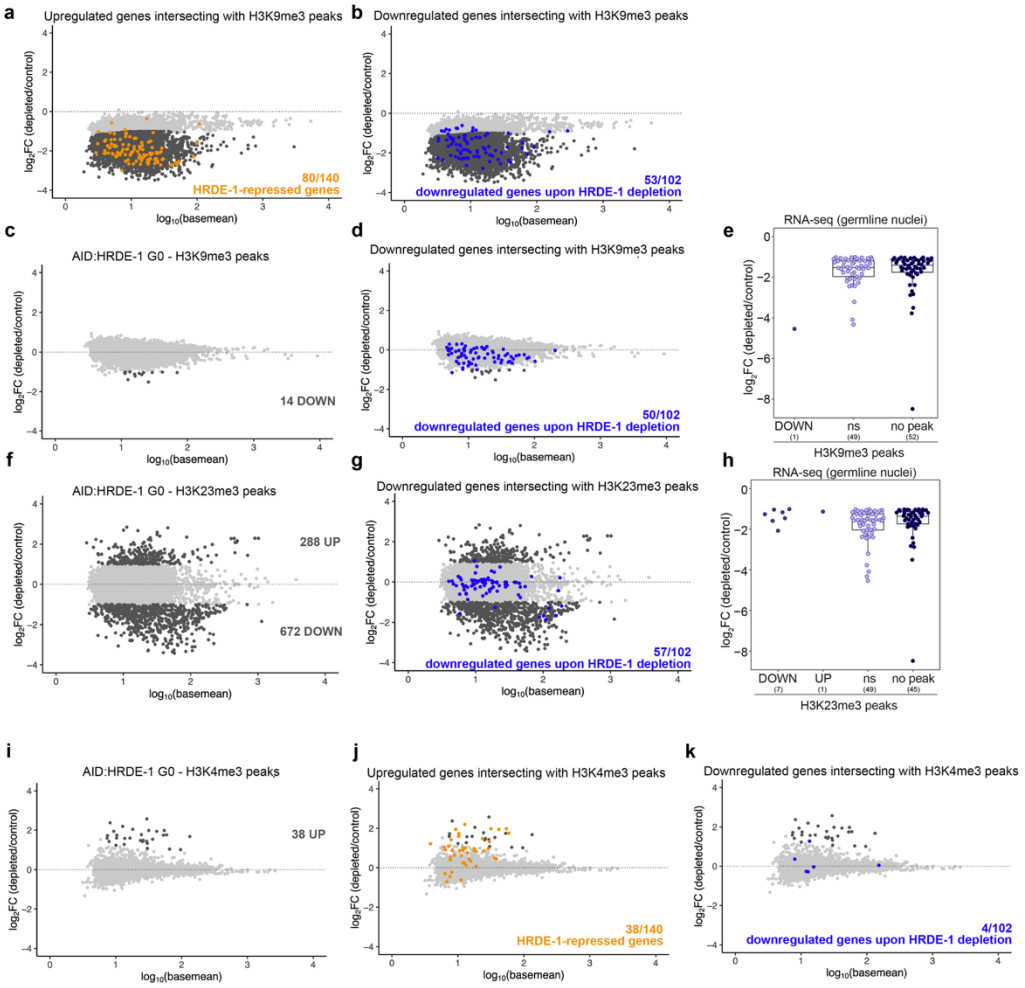

Ext. Data Figure 5

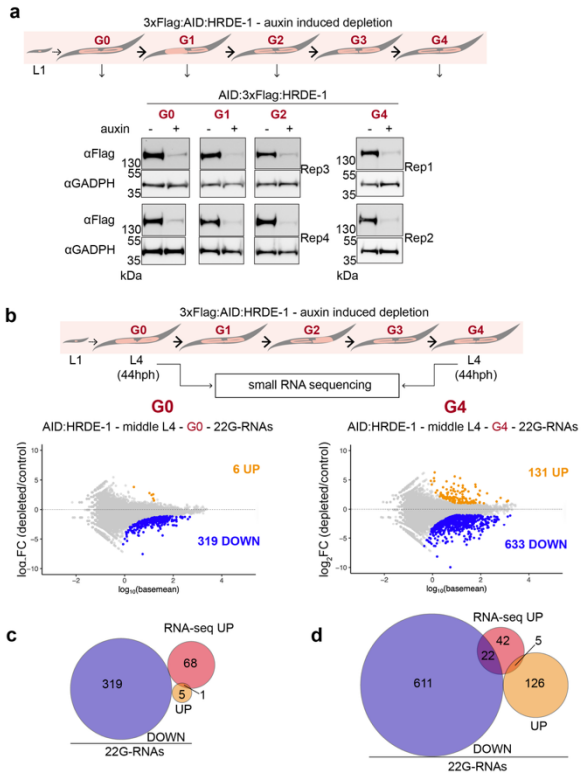

Ext. Data Figure 6

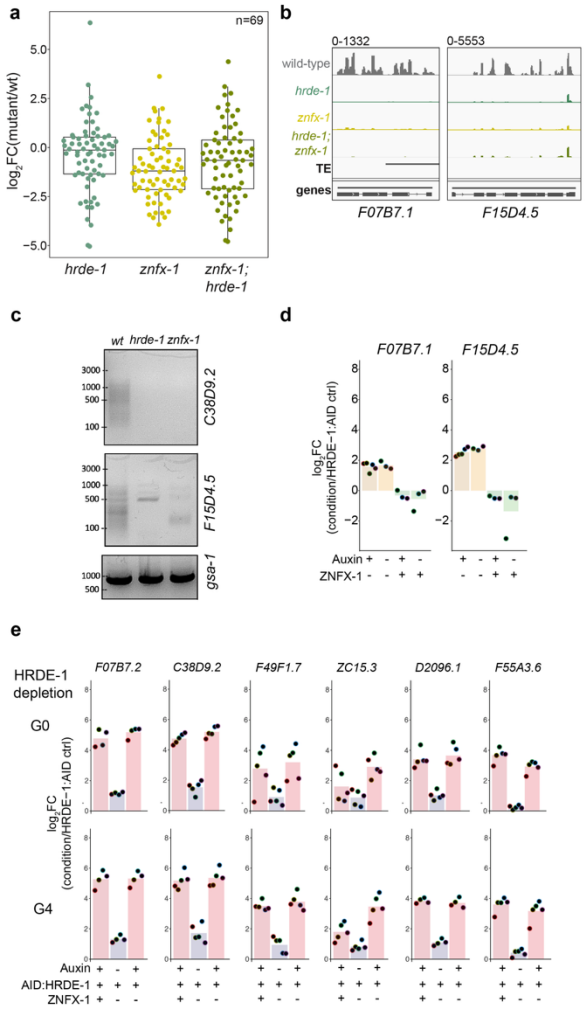
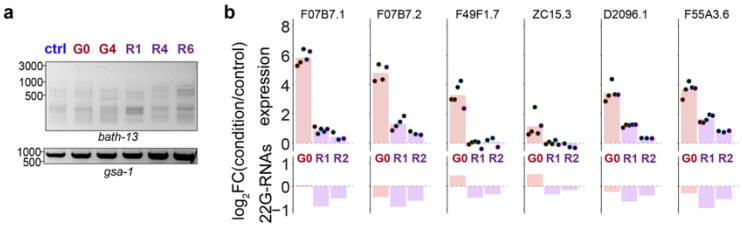
Ext. Data Figure 7